NACA

RESEARCH MEMORANDUM

FLIGHT INVESTIGATION OF THE TRANSONIC LONGITUDINAL AND LATERAL HANDLING QUALITIES OF THE DOUGLAS X-3 RESEARCH AIRPLANE

By Jack Fischel, Euclid C. Holleman, and Robert A. Tremant

High-Speed Flight Station
Edwards, Calif.

NATIONAL ADVISORY COMMITTEE
FOR AERONAUTICS

WASHINGTON

December 5, 1957

NATIONAL ADVISORY COMMITTEE FOR AERONAUTICS

RESEARCH MEMORANDUM

FLIGHT INVESTIGATION OF THE TRANSONIC LONGITUDINAL AND LATERAL HANDLING QUALITIES OF THE DOUGLAS X-3 RESEARCH AIRPLANE

By Jack Fischel, Euclid C. Holleman, and Robert A. Tremant

SUMMARY

A flight investigation was performed to determine the longitudinal and lateral handling qualities of the Douglas X-3 research airplane in the clean configuration. Static and dynamic stability and control characteristics were determined during trimmed and maneuvering flight at an average altitude of 30,000 feet and over a Mach number range from 0.7 to 1.16. A limited longitudinal investigation was also performed at Mach numbers up to 0.9 with wing leading-edge flaps moderately deflected.

Longitudinal and lateral control deflections required to trim the airplane in 1g flight varied somewhat over the speed range; however, the pilot did not consider these variations objectionable, and believed the longitudinal trim (speed-stability) characteristics were particularly acceptable. The longitudinal damping characteristics following abrupt control pulses were positive and appeared satisfactory over the entire speed range; however, the lateral damping was poor and generally unsatisfactory.

Mild pitch-ups were experienced at moderate angles of attack over the entire speed range. Pitch-up occurred near maximum wing lift at Mach numbers up to approximately 0.9, but well below the higher levels of maximum wing lift occurring at higher speeds. The low-lift static margin was about 15 percent for Mach numbers below 0.9, and increased to about 40 percent at a Mach number of about 1.1. The stabilizer control effectiveness was essentially constant over the speed range.

An increase in the apparent directional stability parameter $d\delta_r/d\beta$ with increase in Mach number, particularly above a Mach number of 0.95, is directly attributable to the individual trends over the Mach number range of the directional stability parameter C_{n_β} and the rudder control

effectiveness parameter $C_{n_{\delta_r}}$, which exhibited the usual transonic-supersonic variations. The apparent dihedral parameter $d\delta_a/d\beta$ was almost constant below a Mach number of 0.9, decreased to a value near zero at a Mach number of 1.0, then increased to about one-half the subsonic value at a Mach number of 1.09. The effective dihedral parameter C_{l_β} had a minimum value at a Mach number of 0.95, with appreciably higher values at higher and lower Mach numbers. Both the trimmed lateral-force parameter C_{Y_β} and the damping-in-roll parameter C_{l_p} had essentially constant values over the Mach number range.

The aileron and the rudder controls exhibited typical transonic decreases in effectiveness at Mach numbers above approximately 0.9; the ailerons exhibited favorable yawing-moment characteristics, particularly at speeds below a Mach number of 0.85.

Despite decreases in the aileron rolling effectiveness parameter $\frac{pb}{2V}/\delta_a$ with increase in speed, the pilot thought that the rolling characteristics were satisfactory, except for the violent roll coupling experienced.

Essentially similar longitudinal characteristics were determined with wing leading-edge flaps retracted and deflected.

INTRODUCTION

The Douglas X-3 research airplane was provided for the National Advisory Committee for Aeronautics by the U. S. Air Force to investigate the transonic and supersonic characteristics of an airplane having a thin, straight, low-aspect-ratio wing with hexagonal sections. The airplane is characterized by a long fuselage with a large ratio of frontal area to wing area. With the two turbojet engines and afterburners with which it was equipped, the airplane was limited to near-sonic speeds in level flight, although supersonic speeds could be attained by diving.

Limited stability and control characteristics and performance characteristics of the airplane determined during the manufacturer's demonstration and U. S. Air Force evaluation flights have been reported in references 1 and 2, respectively. Buffeting characteristics and wing- and tail-loads characteristics determined during the subsequent NACA flight test program have been reported in references 3 to 6. This paper presents the more complete longitudinal and lateral handling qualities of the airplane determined during the NACA tests at Mach numbers above approximately 0.7 and at an altitude of about 30,000 feet. Limited data

[redacted]

are also presented for the longitudinal stability and control characteristics of the airplane with the wing leading-edge flaps deflected 6° to 11°, the true deflection varying with flap load.

Inasmuch as the 1 g stall characteristics measured for several leading- and trailing-edge-flap configurations during NACA tests are essentially similar to the characteristics determined during the demonstration tests reported in reference 1, these data are not presented herein.

SYMBOLS

All coefficients and moments of inertia are referenced to the body axes.

a_t	transverse acceleration, g units
a_n	normal-load factor or acceleration, g units
b	wing span, ft
C_l	airplane rolling-moment coefficient
C_{l_p}	damping-in-roll derivative, $\frac{dC_l}{d\left(\frac{pb}{2V}\right)}$, per radian
C_{l_r}	variation of rolling-moment coefficient with yawing angular velocity factor, $\frac{dC_l}{d\left(\frac{rb}{2V}\right)}$, per radian
C_{l_β}	variation of rolling-moment coefficient with sideslip angle, per deg
$C_{l_{\delta_a}}$	variation of rolling-moment coefficient with total aileron deflection, per deg
$C_{l_{\delta_r}}$	variation of rolling-moment coefficient with rudder deflection, per deg
C_m	airplane pitching-moment coefficient
$C_{m_{C_N}}$	variation of pitching-moment coefficient with normal-force coefficient (airplane static margin)

[redacted]

$C_{m_{i_t}}$ variation of pitching-moment coefficient with stabilizer deflection, per deg

$C_{m_q} + C_{m_{\dot{\alpha}}}$ pitch-damping derivative, $\frac{dC_m}{d\left(\frac{q\bar{c}}{2V}\right)} + \frac{dC_m}{d\left(\frac{\dot{\alpha}\bar{c}}{2V}\right)}$, per radian

C_{m_α} variation of pitching-moment coefficient with angle of attack, per deg

C_N airplane normal-force coefficient, $a_n W/q_0 S$

C_{N_α} slope of airplane normal-force-coefficient curve, per deg

C_n airplane yawing-moment coefficient

C_{n_p} variation of yawing-moment coefficient with rolling angular velocity factor, $\frac{dC_n}{d\left(\frac{pb}{2V}\right)}$, per radian

C_{n_r} damping-in-yaw derivative, $\frac{dC_n}{d\left(\frac{rb}{2V}\right)} - \frac{dC_n}{d\left(\frac{\dot{\beta}b}{2V}\right)}$, per radian

C_{n_β} variation of yawing-moment coefficient with sideslip angle, per deg

$C_{n_{\delta_a}}$ variation of yawing-moment coefficient with total aileron deflection, per deg

$C_{n_{\delta_r}}$ variation of yawing-moment coefficient with rudder deflection, per deg

C_Y lateral-force coefficient, $a_t W/q_0 S$

C_{Y_β} slope of lateral-force-coefficient curve per degree of sideslip angle

$C_{1/2}$ cycles to damp to one-half amplitude of lateral oscillation

$C_{1/10}$ cycles to damp to one-tenth amplitude of longitudinal oscillation

c wing chord, in.

$\bar{c}$ mean aerodynamic chord, ft

[redacted]

F_a	aileron control wheel force, lb
F_a/δ_a	variation of aileron wheel force with aileron deflection, lb/deg
F_r	rudder pedal force, lb
F_r/δ_r	variation of rudder pedal force with rudder deflection, lb/deg
$dF_r/d\beta$	rate of change of rudder pedal force with sideslip angle, lb/deg
F_s	stabilizer control column force, lb
F_s/i_t	variation of stabilizer control force with stabilizer deflection, lb/deg
dF_s/da_n	rate of change of stabilizer control force with normal acceleration, lb/g
g	acceleration due to gravity, ft/sec^2
h_p	pressure altitude, ft
I_X	moment of inertia about X-axis, $slug\text{-}ft^2$
I_{XZ}	product of inertia, $\frac{1}{2}(I_Z - I_X)\sin 2\epsilon$, $slug\text{-}ft^2$
I_Y	moment of inertia about Y-axis, $slug\text{-}ft^2$
I_Z	moment of inertia about Z-axis, $slug\text{-}ft^2$
i_t	stabilizer deflection with respect to fuselage horizontal reference line, leading edge of stabilizer up is positive, deg
di_t/da_n	rate of change of stabilizer position with normal acceleration, deg/g
di_t/dC_N	apparent longitudinal stability parameter, deg
M	free-stream Mach number
P	period of longitudinal or lateral oscillation, sec
p	rolling angular velocity, radians/sec

[redacted]

$\dot{p}$	rolling angular acceleration, radians/sec^2
p_0	free-stream static pressure, lb/sq ft
$pb/2V$	wing-tip helix angle, radians
$\frac{pb/2V}{\delta_a}$	variation of wing-tip helix angle with total aileron deflection, radians/deg
q	pitching angular velocity, radians/sec
$\dot{q}$	pitching angular acceleration, radians/sec^2
q_0	free-stream dynamic pressure, lb/sq ft
r	yawing angular velocity, radians/sec
$\dot{r}$	yawing angular acceleration, radians/sec^2
S	wing area, sq ft
$T_{1/2}$	time to damp to one-half amplitude of longitudinal or lateral oscillation, sec
t	time, sec
V	true airspeed, ft/sec
v_e	equivalent side velocity, ft/sec
W	airplane weight, lb
α	angle of attack relative to fuselage horizontal reference plane, deg
$\dot{\alpha}$	rate of change of angle of attack, radians/sec
β	angle of sideslip, deg
$\dot{\beta}$	rate of change of angle of sideslip, radians/sec
δ_a	total aileron deflection, right roll positive, deg
$d\delta_a/d\beta$	apparent effective dihedral parameter
δ_r	rudder deflection, deg
$d\delta_r/d\beta$	apparent directional stability parameter

[redacted]

$\delta_{f_{le}}$ wing leading-edge-flap deflection, deg

δ_{w_s} stabilizer control column travel, in.

ϵ angle between body X-axis and principal X-axis, positive when body axis is above principal axis at airplane nose, deg

φ angle of bank, deg

DESCRIPTION OF AIRPLANE

The Douglas X-3 research airplane is a single-place straight-wing airplane powered by two J34 turbojet engines equipped with afterburners. The airplane is characterized by a long fuselage with an appreciable ratio of frontal area to wing area. Photographs of the airplane are shown in figures 1 and 2. A three-view drawing is presented in figure 3. Additional airplane physical characteristics are given in table I. Figure 4 shows the variation of the moment of inertia about the body axes based on the manufacturer's estimates for weight conditions expected in the normal flight range. The low midwing has an aspect ratio of 3.1, is unswept at the 75-percent-chord line, and is equipped with both leading- and trailing-edge flaps. The constant-chord wing leading-edge flaps were undeflected for most of this investigation; however, limited tests were performed with a selected flap deflection of 10°, the true deflection varying between 6° and 11°, depending on flap load. The airfoil employed for the wing is a 4.5-percent-thick modified hexagonal section.

The airplane has an all-movable horizontal-tail surface and conventional flap-type rudder and aileron control surfaces. The aerodynamic control surfaces are powered by an irreversible hydraulic system and have variable artificial force gradients. The horizontal tail has fixed tabs to alleviate the stick forces due to hinge moments if a hydraulic system failure should occur. Preloaded springs are used in the control system to provide a variation of control force with control deflection. A dynamic-static pressure-sensing unit changes the mechanical advantage between the cockpit controls and the feel springs, producing control-force gradients as shown in figure 5.

Provision is also included for varying stabilizer control-force gradients provided by the preloaded springs independent of the dynamic-static pressure-sensing unit. However, the automatic dynamic-static pressure-sensing unit was used throughout the present investigation to govern the control forces. Both breakout and friction forces are prevalent

[redacted]

in the control system (for example, fig. 5(c)) and the control-force friction appears to increase somewhat with increase in the control-force gradient $\left(F_s/i_t\right)$.

INSTRUMENTATION

The following pertinent quantities were recorded on NACA internal recording instruments which were synchronized by a common timer:

Airspeed and altitude
Normal and transverse acceleration
Rolling angular velocity and acceleration
Pitching angular velocity and acceleration
Yawing angular velocity and acceleration
Angle of attack and angle of sideslip
Control column, control wheel, and rudder pedal positions
Stabilizer, aileron, and rudder positions
Stabilizer, aileron, and rudder control forces
Leading- and trailing-edge-flap positions

An NACA high-speed pitot-static tube was mounted on the airplane nose boom to measure the airspeed and altitude. The airspeed system was calibrated in flight and the accuracy of Mach number measurement from the airspeed calibration is estimated to be within ±0.01. The vanes used to measure the angle of attack and the angle of sideslip were also mounted on the nose boom as shown in figures 1 and 2. The values presented for angle of attack and angle of sideslip were not corrected for the effects of upwash or sidewash, respectively, nor for the effects of boom bending or angular velocity. The angular velocities encountered were not sufficiently high to change the results appreciably.

TESTS

Measurements of the longitudinal and lateral handling qualities of the X-3 airplane, both in the clean configuration and with wing leading-edge flaps deflected, were made at center-of-gravity positions between 3 percent and -2 percent of the wing mean aerodynamic chord. A more precise determination or selection of the center-of-gravity position was limited by the existing instrumentation (pertinent to fuel consumption) and by the configuration of fuel tanks in the airplane. In general, the data were obtained with wing leading-edge flaps undeflected at speeds ranging from $M \approx 0.7$ to $M \approx 1.16$ and at pressure altitudes from 25,000 to 35,000 feet. With wing leading-edge flaps deflected, tests were limited to $M \lesssim 0.9$ by flap design loads.

[redacted]

Longitudinal and lateral trim data were obtained from stall approaches, level-flight speed runs, and dives. Static longitudinal stability and control characteristics were determined during push-down wind-up turn maneuvers; static lateral stability and control characteristics were determined from gradually increasing right and left constant-heading sideslips; lateral-control effectiveness was determined from abrupt rudder-fixed aileron rolls at various aileron deflections. Only limited aileron deflections were used during the later phases of the roll test program because of violent lateral-longitudinal coupling encountered when large aileron deflections were used during the earlier phases (ref. 7). Dynamic longitudinal and lateral stability characteristics were determined from stabilizer and rudder pulses, respectively, initiated from 1 g level-flight conditions.

RESULTS AND DISCUSSION

Longitudinal Stability and Control

Longitudinal trim.- Figure 6 presents the trim force and stabilizer variations over the Mach number range from $M = 0.6$ to 1.16, corrected to conditions of 1 g flight at an altitude of 30,000 feet and for a wing loading of 116 pounds per square foot. The stick-free and stick-fixed characteristics exhibit similar trends over the speed range covered and appear stable, except in the region between $M = 0.9$ and 0.97 and above $M \approx 1.1$ where neutral to slightly unstable regions are shown. However, the pilot experienced no difficulty with these neutral to slightly unstable regions, nor with the sudden increase in stability in the region between $M \approx 0.97$ and 1.05, and considered the trim characteristics of the airplane quite acceptable, especially when compared to other airplanes exhibiting appreciable unstable trim characteristics in the transonic region.

The effects of deflecting the wing leading-edge flaps on the trim characteristics of the airplane were negligible for the comparable speed range covered.

Dynamic longitudinal stability.- The dynamic longitudinal stability characteristics of the airplane were investigated by initiating stabilizer-pulse maneuvers from 1 g flight conditions, corresponding to the values of C_N shown as a function of Mach number in figure 7. Time histories of two typical maneuvers are shown in figure 8. The data of figure 7 show that the pulses at the two lowest speeds were obtained in the airplane buffet region, hence the characteristics of the oscillation and the airplane stability may differ somewhat from those at the higher speeds.

[redacted]

However, for all pulse maneuvers performed, the oscillations of the airplane with controls fixed were well damped and essentially disappeared after about 2 to 3 cycles.

The characteristics of the longitudinal oscillations experienced with the X-3 airplane are presented as a function of Mach number in figure 9. The period P decreases quite rapidly from 3.75 seconds at $M = 0.78$ to 2 seconds at $M \approx 0.91$, remains fairly constant to $M \approx 0.96$, then decreases slowly to about 1.5 seconds at $M = 1.11$. As might be anticipated, the values of P obtained in the buffet region at the two lowest speeds exhibit markedly different trends from those obtained at slightly higher speeds. The values of $T_{1/2}$ decrease steadily to $M \approx 0.96$, then remain fairly constant with further increase in speed. From the variation with Mach number of the values of $C_{1/10}$, it is apparent that the airplane does not satisfy the amended longitudinal requirements of reference 8 for damping to one-tenth amplitude within 1 cycle of the oscillation. The pilot reported the airplane exhibited satisfactory dynamic characteristics following abrupt control pulses at all speeds, and that the damping was always positive. The pilot also reported, however, that the airplane exhibited poor dynamic characteristics in normal flying below $M = 1.0$, as discussed in the next section.

Static longitudinal stability.- Time histories of several typical accelerated longitudinal maneuvers performed at essentially constant Mach numbers with wing leading-edge flaps neutral and deflected are presented in figure 10. These data are also presented in the form of stability cross plots in figure 11 to illustrate the relative variations of the quantities measured. The variations of airplane pitching-moment coefficient with angle of attack shown in figure 11 were obtained by reducing the flight data by an analysis similar to that employed in reference 9. In general, the maneuvers performed at $M \lesssim 0.9$ were over a lift range extending into the buffet region and up to or near wing maximum lift ($C_N \approx 0.6$ to 0.7, ref. 3). At $M \gtrsim 0.9$ the maneuvers were performed over a much larger lift range, extending as high as $C_N \approx 1.2$. In general, higher values of C_N were attained with wing leading-edge flaps deflected than in the retracted condition.

The time histories of figure 10 reveal that the movements of the stabilizer control wheel and the stabilizer surface are in phase and exhibit an almost negligible lag; whereas, both these quantities seem to lag the changes in control force occurring during each maneuver. These effects result from control-force breakout and friction (static and valve) which were noted in the control system (as discussed in DESCRIPTION OF AIRPLANE). In addition, the data of figure 10 show that changes in angle of attack appear to lag appreciably, then overshoot

the corresponding changes in F_s and i_t. These effects are believed to result principally from the airplane and control system dynamics and from changes in static stability over the angle-of-attack range (discussed in the following paragraph). As a result of these effects, and their effects on pilot control input, the maneuvers shown in figure 10, as well as others performed, seem somewhat oscillatory in nature over the lift range.

Some of these effects may be observed more clearly in the cross plots of figure 11, which show the linear and nonlinear variations of the stability measurements. Using the equation

$$\Delta i_t = \frac{I_Y \dot{q}}{q_O S \bar{c} C_{m_{i_t}}}$$

to correct the values of i_t (shown in fig. 11 plotted against α and C_N) to a condition of $\dot{q} = 0$, the low-lift static stability appears more linearized, and a decrease in the static stability at higher levels of C_N and α becomes quite apparent. At $M \lesssim 1.0$ (figs. 11(a), (b), (d), and (e)) the decrease in stability was somewhat abrupt and was reported as a pitch-up by the pilot; however, because of the proximity to maximum wing lift at $M \lesssim 0.9$ (ref. 3) the airplane did not pitch to any great extent, and at speeds between $M \approx 0.9$ and 1.0 the pitch rate during the pitch-up was generally quite low (less than 0.3 radian/sec). At supersonic speeds, the decrease in stability was gradual, followed by a pitch-up which was characterized by generally low pitch rates. In addition, the pitch-up at the higher speeds was occasionally accompanied by a roll-off or "snap roll," which tended to make the pitch-up more objectionable to the pilot. To indicate clearly the levels of α and C_N at which the decrease in longitudinal stability occurred, a vertical tick is shown in figure 11 on the plots of i_t (corrected to $\dot{q} = 0$) against α and C_N, and C_m plotted against α. The variations with Mach number of these values of α and C_N are shown in figure 12. The value of C_N for the decrease in stability occurs at approximately 0.6 for $M \lesssim 0.9$, increases to about 0.85 at $M \approx 0.99$, then decreases to about 0.6 at $M \approx 1.04$, and remains essentially constant to $M \approx 1.15$, the limit of these results. It should be noted (fig. 11) that the values of C_N at which the decrease in stability occurred correspond to the attitudes where neutral static stability was exhibited for $M \lesssim 0.99$, whereas at higher speeds, neutral stability occurred at appreciably higher angles of attack, corresponding to $C_N \approx 0.8$ to 0.9.

The nonlinear character of the stick-force variation with acceleration is shown in figure 11, thereby indicating the maneuvering difficulties (previously discussed) which are thought to be attributable mainly to the friction and breakout forces in the control-feel system. The data of figures 10 and 11 show that a decrease in stick-free stability generally preceded the decrease in stick-fixed stability, and at high angles of attack stick-free instability was apparent.

In general, there are no significant differences in stability characteristics between wing leading-edge-flap-retracted or deflected configurations.

Longitudinal stability and control effectiveness parameters.- Figure 13 presents the variation with Mach number of the stability and control effectiveness parameters. These quantities were determined from wind-up turns (in the low-lift region) and from stabilizer pulses. The static stability parameter C_{m_α} was computed using the period and damping data of figure 9 in the expression

$$C_{m_\alpha} = -\frac{I_Y}{(57.3)q_0 S\bar{c}}\left[\left(\frac{2\pi}{P}\right)^2 + \left(\frac{0.693}{T_{1/2}}\right)^2\right]$$

Values of the static margin $C_{m_{C_N}}$ were calculated by combining the values of C_{m_α} and C_{N_α} determined from pulse maneuvers. The control effectiveness parameter $C_{m_{i_t}}$ was determined from abrupt stabilizer pulses using the acceleration method similar to that described in reference 10.

Over the speed range investigated, the values of C_{N_α} determined from wind-up turn and stabilizer-pulse maneuvers are in good agreement and exhibit the characteristic subsonic rise and supersonic decrease with increase in Mach number. The variations with Mach number of the airplane static margin $C_{m_{C_N}}$ and the apparent static stability parameter di_t/dC_N were quite similar except near $M \approx 0.91$, indicating that most of the increase in apparent stability with increase in Mach number resulted from an increase in airplane stability. This is verified by the almost constant values of the control effectiveness parameter $C_{m_{i_t}}$ (approximately -0.037 per deg) determined over the speed range, except for the inflection values noted near $M \approx 0.91$. It will be noted in figure 13 that the static margin was approximately 15 percent for

$M \lessapprox 0.9$ and increased appreciably with Mach number to a value of about 40 percent at $M \approx 1.1$.

A rather small variation with Mach number of the stick-force parameter dF_s/da_n is evident in figure 13, where essentially constant values of dF_s/da_n at speeds above and below $M = 0.95$ can be seen. These effects probably result from the compensating effects of the variations of F_s/i_t (fig. 5) and di_t/da_n with increase in Mach number. These variations of dF_s/da_n with Mach number differ appreciably from those previously presented in reference 1, inasmuch as the automatic pressure-sensing load-feel unit was used in the present investigation, and manual load feel (only a spring arrangement) was used in the reference investigation.

With wing leading-edge flaps deflected, slightly lower values of C_{N_α} were obtained at $M > 0.8$, and negligibly lower values of di_t/dC_N and dF_s/da_n were obtained at all speeds than with the flaps retracted. However, the trends shown for both configurations were similar. The effects of flap deflection on C_{N_α} were similar to those reported in reference 11.

Lateral Stability and Control

Lateral trim.- The variations with Mach number of the rudder and aileron positions required to trim the airplane at a sideslip angle of 0° are shown in figure 14. Although the absolute values of the control positions required for trim varied to some degree for different flights performed, the general trend shown in figure 14 represents an average of actual variations measured. As Mach number increased to 1.0, the airplane required a small amount of left rudder; however, this trend reversed at $M \approx 1.0$ so that about 1.5° of right rudder was required at $M \approx 1.16$. The amount of right aileron position required increased with an increase in Mach number abruptly at $M \approx 0.93$. At this point when left-wing drop became quite apparent and the aileron effectiveness decreased, the amount of right aileron deflection required to hold wings level reached a peak value of about 3°. At $M \gtrapprox 0.93$ the amount of right aileron required decreased as Mach number increased, and at $M \approx 1.16$ a slight degree of left aileron was required.

Dynamic lateral stability.- The dynamic lateral stability characteristics of the airplane were investigated by initiating rudder-pulse maneuvers from 1 g flight conditions. Time histories of two typical maneuvers are shown in figure 15. At all speeds investigated, the

lateral oscillations were poorly damped and involved pitching as well as yawing and rolling motions. The slight pitching motions probably resulted from aerodynamic and engine gyroscopic coupling.

The characteristics of the lateral oscillations of the X-3 airplane are presented as a function of Mach number and of the ratio of bank angle to equivalent side velocity in figure 16. Although data obtained were not sufficient to define completely the characteristics of the oscillations in the two altitude regions shown and over the entire test Mach number range, the usual decreases in the period of the lateral oscillation with increase in speed or decrease in altitude are evident. The effects of changes in altitude or Mach number on the values of $T_{1/2}$ appear to be poorly defined, probably because of the poor damping. From a comparison of the flight test data on the basis of $\frac{1}{C_{1/2}}$ plotted against $\frac{\varphi}{v_e}$ with the Military Specification for dynamic lateral stability (ref. 8), it is evident that the airplane provides unsatisfactory lateral stability over essentially the entire speed range. Pilot opinion generally concurred in this unsatisfactory dynamic stability rating, although some tolerable (less unsatisfactory) ratings were given to several of the maneuvers performed at the higher speeds.

Static lateral stability.- Representative cross-plots of data obtained during constant-heading sideslips plotted against angle of sideslip are presented in figure 17. The scatter in the data results from the almost continuous oscillations experienced during the sideslips.

The results obtained show that a slight nose-down pitching moment was experienced at the lower speeds for the larger angles of sideslip attained, but at higher speeds this effect disappeared. The variations with sideslip angle of both δ_r and δ_a generally were reasonably linear at all speeds, as was the variation of the lateral-force coefficient C_Y. An appreciable breakout pedal force, with little or no accompanying variations in β, is observed for each typical maneuver in figure 17. The pedal force exhibits a reasonably linear variation with β beyond the breakout and friction level.

Lateral stability and control effectiveness parameters.- Data obtained during the previously discussed sideslip maneuvers are summarized in figure 18 as the variations over the Mach number range of the stick-free directional stability parameter $dF_r/d\beta$, the apparent directional stability parameter $d\delta_r/d\beta$, the apparent dihedral parameter $d\delta_a/d\beta$, and the trimmed lateral-force derivative C_{Y_β}. In general, the values of these quantities show good agreement for left and right

[redacted]

sideslip maneuvers. The values of $d\delta_r/d\beta$ changed only slightly subsonically, increasing from a value of about 1.3 at $M = 0.75$ to a value of about 1.5 at $M = 0.95$, then increased more rapidly with increase in Mach number to a value of 2.3 at $M = 1.09$. These changes reflect either an increase in directional stability, a decrease in rudder effectiveness, or a combination of these two effects as Mach number increases (as will be discussed subsequently). The variations with Mach number of $dF_r/d\beta$ essentially agree with the trends exhibited by the parameter $d\delta_r/d\beta$. Although the apparent dihedral parameter is almost constant at a value near 0.9 at speeds below $M \approx 0.9$, it decreases to a value of about 0.1 at $M \approx 1.0$, then increases to about 50 percent of the subsonic value at $M \approx 1.09$. Over the Mach number range investigated, C_{Y_β} remained essentially constant at a value of about -0.012 per degree.

The variations with Mach number of the lateral stability parameters C_{n_β}, C_{n_r}, C_{n_p}, C_{l_p}, C_{l_β}, and C_{l_r} are shown in figure 19. The faired curves shown for C_{n_p} and C_{l_r} were estimated for the airplane by Douglas Aircraft Co. The flight data presented were determined from rudder-pulse maneuvers by the vector-analysis method of reference 12 using the values of C_{l_r} and C_{n_p} shown in figure 19. Despite some scatter in the flight data, fairly definite trends are apparent. The directional stability parameter C_{n_β} exhibits typical transonic changes, increasing from a value of about 0.0015 per degree at $M = 0.7$ to an apparent peak value of about 0.0038 per degree at $M = 1.1$. However, little change in C_{n_β} is indicated in the range above $M \approx 1.0$. Comparison of the values of C_{n_β} determined by the usual period-damping relationship $\left(\text{including the effects of } C_{l_\beta}\right)$ with the values of C_{n_β} given herein for the vector-analysis method showed good agreement. With increase in Mach number, C_{n_r} decreased appreciably to a minimum value of about -0.9 at $M = 0.95$, then increased to about -1.6 at $M = 1.16$. The test points shown for C_{l_p} indicate an average value of about -0.38 per radian existed over most of the speed range; however, C_{l_p} appeared to decrease to a minimum value of less than -0.3 per radian near $M \approx 0.95$. The airplane effective dihedral parameter C_{l_β} decreased from a value of about -0.0012 per degree at $M = 0.7$ to a minimum value of -0.0006 per degree at $M = 0.95$, followed by an increase to a value of -0.0008 per degree at $M > 1.1$. This trend was somewhat similar to that exhibited by the variations of $d\delta_a/d\beta$ with Mach number (fig. 18).

[redacted]

The control-effectiveness parameters $C_{n_{\delta_r}}$, $C_{l_{\delta_r}}$, $C_{l_{\delta_a}}$, and $C_{n_{\delta_a}}$ were determined from abrupt rudder-pulse maneuvers and abrupt rudder-fixed aileron roll maneuvers by the acceleration method discussed in reference 10. Values of these parameters at speeds from $M = 0.7$ to 1.16 are presented in figure 20. Both $C_{n_{\delta_r}}$ and $C_{l_{\delta_r}}$ exhibit essentially similar trends with increase in speed; the rudder effectiveness parameter $C_{n_{\delta_r}}$ remained constant at about -0.002 up to $M = 0.95$, then decreased to half this value at $M = 1.15$, whereas $C_{l_{\delta_r}}$ remained at approximately 0.00021 up to $M \approx 1.0$, then decreased to 0.00013 at $M \approx 1.15$. The aileron effectiveness parameter $C_{l_{\delta_a}}$ increased with Mach number subsonically to a peak value of 0.0008 at $M \approx 0.87$, and decreased gradually with increase in Mach number above $M \approx 0.98$ to the minimum measured value of $C_{l_{\delta_a}} \approx 0.00045$ at $M = 1.15$. However, an abrupt decrease in aileron effectiveness is indicated in the region of $M \approx 0.92$, where a value of $C_{l_{\delta_a}} \approx 0.00045$ was realized. The ailerons provided appreciable and essentially constant favorable values of the yawing-moment parameter $C_{n_{\delta_a}}$ at $M < 0.85$; these values of $C_{n_{\delta_a}}$ decreased appreciably between $M \approx 0.85$ and 0.92, and were small, though constant and favorable, at $M > 0.92$.

The variations over the Mach number range of C_{n_β} and $C_{n_{\delta_r}}$ discussed in the preceding paragraphs are shown to account for the trends previously noted for the apparent directional stability parameter $d\delta_r/d\beta$ (fig. 18). At $M \approx 0.95$, the slight increase of $d\delta_r/d\beta$ with Mach number is attributable to the increase in directional stability C_{n_β}, inasmuch as $C_{n_{\delta_r}}$ is constant. At $M > 0.95$, the increases in $d\delta_r/d\beta$ with Mach number are attributable mainly to the decrease in control effectiveness $C_{n_{\delta_r}}$, since the directional stability appears to change only slightly in this speed range.

Lateral control.- The lateral control characteristics of the airplane were determined by performing, at specified speeds, abrupt rudder-fixed aileron rolls at various deflections. As a result of the violent lateral-longitudinal coupling encountered during large-deflection aileron rolls early in this program (ref. 7), only small and moderate aileron deflections were utilized during the later phases of the testing. Typical variations of the wing-tip helix angle $pb/2V$ generated during the

rolls are plotted as a function of aileron deflection in figure 21. In general, the variation of $pb/2V$ with δ_a was observed to be linear over the test ranges.

The variation with Mach number of the lateral control effectiveness parameter per degree of aileron deflection $\frac{pb}{2V}\Big/\delta_a$ is shown in figure 22. The value of $\frac{pb}{2V}\Big/\delta_a$ decreased from about 0.00245 at $M = 0.75$ to about 0.0015 at $M = 1.13$; most of this decrease occurred below $M \approx 0.93$. It will be noted that the variation of $\frac{pb}{2V}\Big/\delta_a$ with Mach number at $M > 0.88$ resembles the variation of $C_{l_{\delta_a}}$ over the same speed range, including the inflection point at $M \approx 0.93$. This is not unusual, considering the essentially constant values of C_{l_p} over the entire speed range, except near $M \approx 0.95$. At speeds below $M \approx 0.88$, the variations of $C_{l_{\delta_a}}$ and $\frac{pb}{2V}\Big/\delta_a$ with Mach number are opposite, despite essentially constant values of C_{l_p}. However, in this speed range, the aileron yawing moments are appreciable and probably affect the peak roll rates obtained and used in evaluating the parameter $\frac{pb}{2V}\Big/\delta_a$.

The pilot considered the airplane acceleration in roll satisfactory and the airplane rolling velocities, even at supersonic speeds, more than adequate. However, he did object vociferously to the violent motions experienced during the inertial-roll-coupling maneuvers encountered during several large deflection aileron rolls (ref. 7).

To illustrate flight conditions at which the airplane might experience inertial roll coupling, the analytical method of reference 13, in modified form, has been used to calculate the lower resonant frequencies of the X-3 airplane over the flight range. When the average roll velocity in 360° rolls exceeds the lower resonant frequency, undesirably large changes in angle of sideslip or angle of attack might be expected (ref. 14). The approximate flight test envelope of the X-3 airplane, together with lines of constant lower resonant frequency (yaw), is shown in figure 23. Also shown in this figure are the flight conditions at which inertial coupling was experienced during the flight roll program. Large peak roll rates, in excess of the frequencies shown for inertial coupling, have been obtained during the flight test program; however, the average roll frequencies during 360° rolls or the roll

[redacted]

bank angles have been sufficiently low to avert the coupling effects, except as shown in figure 23 and reference 7.

CONCLUSIONS

A flight investigation, performed with the Douglas X-3 research airplane with wing leading-edge flaps retracted and deflected, at an average altitude of about 30,000 feet and over a Mach number range from 0.7 to 1.16, indicated the following:

1. Longitudinal control force and deflection required to trim the airplane in 1 g flight exhibited stable trends over the speed range covered, except in the region between a Mach number of 0.9 and 0.97 and above a Mach number of approximately 1.1, where neutral to slightly unstable trends were apparent. Small deflections of both the rudder and aileron, varying in both magnitude and direction, were required to trim the airplane laterally over the test speed range, and a perceptible left-wing drop was noted at a Mach number of about 0.93.

2. The longitudinal damping characteristics of the airplane with controls fixed were always positive and appeared satisfactory to the pilot; however, the lateral damping was generally rated as unsatisfactory and as contributing to the oscillatory motions in sideslip. The airplane did not satisfy the Military Specification for longitudinal and lateral damping.

3. Reasonably linear lift and longitudinal stability characteristics were exhibited at low angles of attack over the entire speed range; however, at moderate values of lift, the stability decreased and mild pitch-ups ensued at higher lift levels. At Mach numbers up to approximately 0.9, the pitch-up occurred near maximum wing lift, and at higher speeds the pitch-up occurred well below the increased transonic-supersonic levels of maximum wing lift.

4. The slope of the airplane normal-force-coefficient curve C_{N_α} exhibited the characteristic subsonic rise and supersonic decrease in value with increase in Mach number. The apparent static stability parameter di_t/dC_N was essentially constant at the lower speeds and increased with Mach number at a Mach number greater than 0.9. The longitudinal static margin $C_{m_{C_N}}$ was about 15 percent for Mach numbers below 0.9, and increased to about 40 percent at a Mach number of about 1.1; whereas the stabilizer control effectiveness parameter $C_{m_{i_t}}$ was

essentially constant over the speed range tested. The stick-force parameter dF_s/da_n had two generally constant levels at low lift for Mach numbers above and below 0.95.

5. Limited longitudinal stability and control characteristics at Mach numbers below 0.9 determined with wing leading-edge flaps moderately deflected were essentially similar in level and trend to those for the clean airplane.

6. The apparent directional stability parameters $d\delta_r/d\beta$ and $dF_r/d\beta$ exhibited essentially similar trends, increasing in value with increase in Mach number particularly above a Mach number of about 0.95. The apparent dihedral parameter $d\delta_a/d\beta$ was almost constant at a Mach number less than 0.9, decreased to a value near zero at a Mach number of approximately 1.0, then increased to about 50 percent of the subsonic value at a Mach number of about 1.09. The trimmed lateral-force parameter C_{Y_β} exhibited essentially no change with increase in Mach number.

7. The directional stability parameter C_{n_β} increased appreciably in value with increase in subsonic speed, but changed little in the range above a Mach number of about 1.0, and appeared to reach a maximum value near a Mach number of 1.1. The effective dihedral parameter C_{l_β} and the damping-in-yaw parameter C_{n_r} had minimum values at a Mach number of 0.95, with appreciably higher values at lower and higher Mach numbers. Except for a minimum value realized in the region near a Mach number of about 0.95, the damping-in-roll parameter C_{l_p} exhibited an essentially constant value over the test Mach number range.

8. The rudder control effectiveness parameters $C_{n_{\delta_r}}$ and $C_{l_{\delta_r}}$ were essentially constant for Mach numbers below about 0.97, then decreased appreciably with further increase in Mach number. The aileron effectiveness parameter $C_{l_{\delta_a}}$ increased with Mach number to a peak value at a Mach number of about 0.88, then decreased abruptly to about 55 percent of the peak value at a Mach number of about 0.92 and had about this same value at a Mach number of 1.15. The aileron yawing-moment parameter $C_{n_{\delta_a}}$ had an appreciable and constant favorable value at Mach numbers less than 0.85, and a small constant favorable value at Mach numbers greater than 0.92.

[redacted]

9. The value of the apparent aileron effectiveness parameter $\frac{pb}{2V}/\delta_a$ decreased approximately 40 percent as Mach number increased from 0.75 to 1.13, with most of the decrease occurring below a Mach number of about 0.93. The pilot considered the rolling acceleration and rolling velocity satisfactory over the entire speed range, but did not appreciate the violent uncontrolled motions experienced during roll coupling.

High-Speed Flight Station,
National Advisory Committee for Aeronautics,
Edwards, Calif., August 16, 1957.

[redacted]

REFERENCES

1. Day, Richard E., and Fischel, Jack: Stability and Control Characteristics Obtained During Demonstration of the Douglas X-3 Research Airplane. NACA RM H55E16, 1955.

2. Bellman, Donald R., and Murphy, Edward D.: Lift and Drag Characteristics of the Douglas X-3 Research Airplane Obtained During Demonstration Flights to a Mach Number of 1.20. NACA RM H54I17, 1954.

3. Baker, Thomas F., Martin, James A., and Scott, Betty J.: Flight Data Pertinent to Buffeting and Maximum Normal-Force Coefficient of the Douglas X-3 Research Airplane. NACA RM H57H09, 1957.

4. Keener, Earl R., and Jordan, Gareth H.: Wing Loads and Load Distributions Throughout the Lift Range of the Douglas X-3 Research Airplane at Transonic Speeds. NACA RM H56G13, 1956.

5. Stephenson, Harriet J.: Flight Measurements of Horizontal-Tail Loads on the Douglas X-3 Research Airplane. NACA RM H56A23, 1956.

6. Marcy, William L., Stephenson, Harriet J., and Cooney, Thomas V.: Analysis of the Vertical-Tail Loads Measured During a Flight Investigation at Transonic Speeds of the Douglas X-3 Research Airplane. NACA RM H56H08, 1956.

7. NACA High-Speed Flight Station: Flight Experience With Two High-Speed Airplanes Having Violent Lateral-Longitudinal Coupling in Aileron Rolls. NACA RM H55A13, 1955.

8. Anon.: Military Specification - Flying Qualities of Piloted Airplanes. MIL-F-8785 (ASG), Amendment -2, Oct. 17, 1955.

9. Peck, Robert F., and Mitchell, Jesse L.: Rocket-Model Investigation of Longitudinal Stability and Drag Characteristics of an Airplane Configuration Having a 60° Delta Wing and a High Unswept Horizontal Tail. NACA RM L52K04a, 1953.

10. Sisk, Thomas R., Andrews, William H., and Darville, Robert W.: Flight Evaluation of the Lateral Stability and Control Characteristics of the Convair YF-102 Airplane. NACA RM H56G11, 1957.

11. Humphreys, Milton D.: Transonic Aerodynamic Characteristics of an NACA 64A006 Airfoil Section With a 15-Percent-Chord Leading-Edge Flap. NACA RM L53G23, 1953.

[redacted]

12. Wolowicz, Chester H.: Time-Vector Determined Lateral Derivatives of a Swept-Wing Fighter-Type Airplane With Three Different Vertical Tails at Mach Numbers Between 0.70 and 1.48. NACA RM H56C20, 1956.

13. Phillips, William H.: Effect of Steady Rolling on Longitudinal and Directional Stability. NACA TN 1627, 1948.

14. Weil, Joseph, and Day, Richard E.: An Analog Study of the Relative Importance of Various Factors Affecting Roll Coupling. NACA RM H56A06, 1956.

[redacted]

TABLE I.- PHYSICAL CHARACTERISTICS OF THE DOUGLAS X-3 AIRPLANE

Wing:	
Airfoil section	Modified hexagon
Airfoil thickness ratio, percent chord	4.5
Airfoil leading- and trailing-edge angles, deg	8.58
Total area, sq ft	166.50
Span, ft	22.69
Mean aerodynamic chord, ft	7.84
Root chord, ft	10.58
Tip chord, ft	4.11
Taper ratio	0.39
Aspect ratio	3.09
Sweep at 75-percent-chord line, deg	0
Incidence, deg	0
Dihedral, deg	0
Geometric twist, deg	0
Aileron:	
Area rearward of hinge line (each), sq ft	4.04
Span at hinge line (each), ft	3.25
Chord rearward of hinge line, percent wing chord	25
Travel (each), deg	±12
Leading-edge flap:	
Type	Plain
Area (each), sq ft	8.38
Span at hinge line (each), ft	8.916
Chord, normal to hinge line, in.	11.50
Travel, deg	30
Trailing-edge flap:	
Type	Split
Area (each), sq ft	8.61
Span, ft	5.083
Chord, percent wing chord	25
Travel, deg	50
Horizontal tail:	
Airfoil section	Modified hexagon
Airfoil thickness ratio at root chord, percent chord	8.01
Airfoil thickness ratio outboard station 26, percent chord	4.50
Airfoil leading-edge angle, deg	11.96
Airfoil trailing-edge angle, deg	8.77
Total area, sq ft	43.24
Span, ft	13.77
Mean aerodynamic chord, ft	3.34
Root chord, ft	4.475
Tip chord, ft	1.814
Taper ratio	0.405
Aspect ratio	4.38
Sweep at leading edge, deg	21.14
Sweep at trailing edge, deg	0
Dihedral, deg	0
Travel, leading edge up, deg	6
Travel, leading edge down, deg	17
Hinge-line location, percent root chord	46.46

TABLE I.- PHYSICAL CHARACTERISTICS OF THE DOUGLAS X-3 AIRPLANE - Concluded

Vertical tail:	
Airfoil section	Modified hexagon
Airfoil thickness ratio, percent chord	4.5
Airfoil leading- and trailing-edge angles, deg	8.58
Area, sq ft	23.73
Span, ft	5.59
Mean aerodynamic chord, ft	4.69
Root chord, ft	6.508
Tip chord, ft	1.93
Taper ratio	0.292
Aspect ratio	1.315
Sweep at leading edge, deg	45
Sweep at trailing edge, deg	9.39
Rudder:	
Area, rearward of hinge line, sq ft	5.441
Span at hinge line, ft	3.535
Root chord, ft	1.98
Tip chord, ft	1.097
Travel, deg	±20
Fuselage:	
Length including boom, ft	66.75
Maximum width, ft	6.08
Maximum height, ft	4.81
Base area, sq ft	7.94
Power plant:	
Engines	Two Westinghouse J34-WE-17 with afterburners
Rating, each engine:	
Static sea-level maximum thrust, lb	4,850
Static sea-level military thrust, lb	3,370
Airplane weight, lb:	
Basic (without fuel, oil, water, pilot)	16,120
Total (full fuel, oil, water, no pilot)	21,900
Center-of-gravity location, percent mean aerodynamic chord:	
Basic weight - gear down	2.63
Total weight - gear down	4.59
Total weight - gear up	3.91
Inclination of principal axis (below body axis at nose of airplane), deg	3

[redacted]

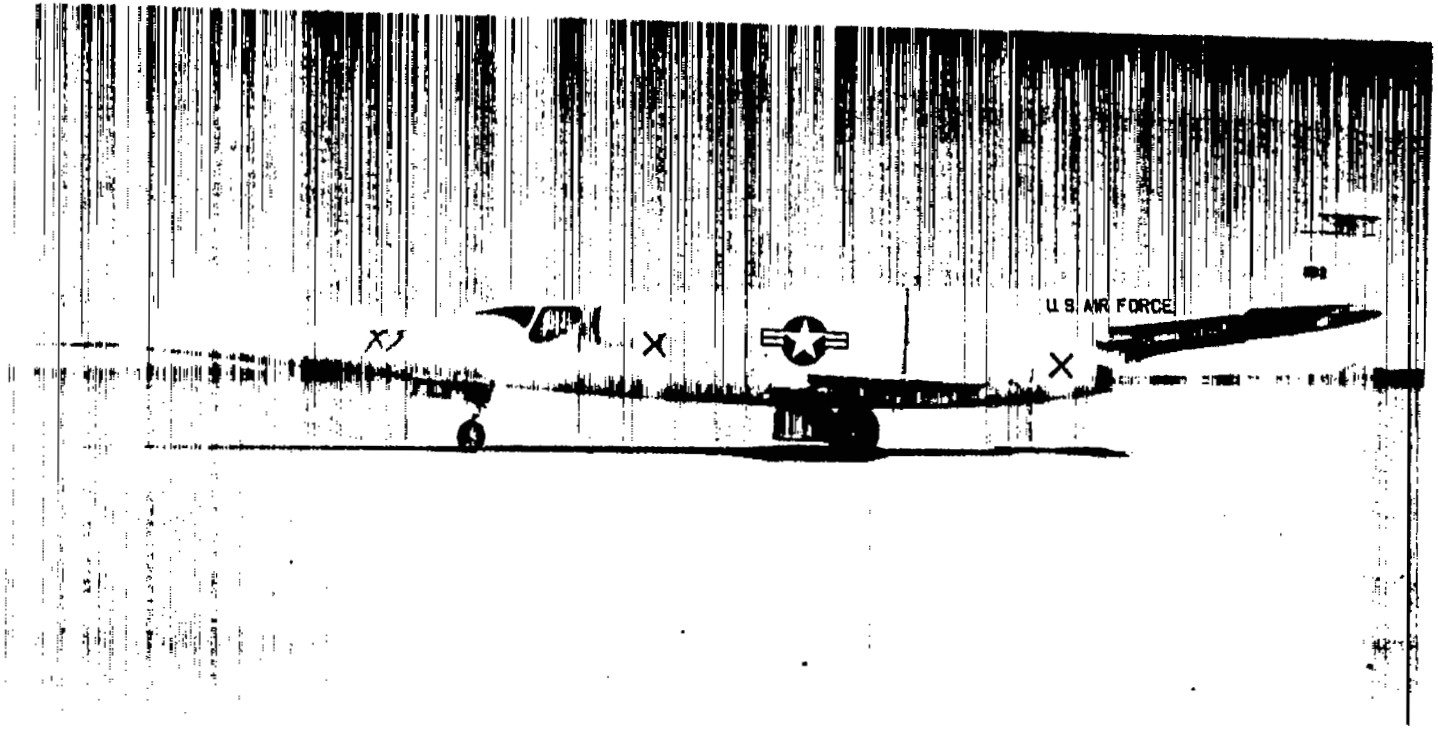

Figure 1.- Side view of Douglas X-3 research airplane. E-1542

Figure 2.- Overhead view of Douglas X-3 research airplane. E-1994

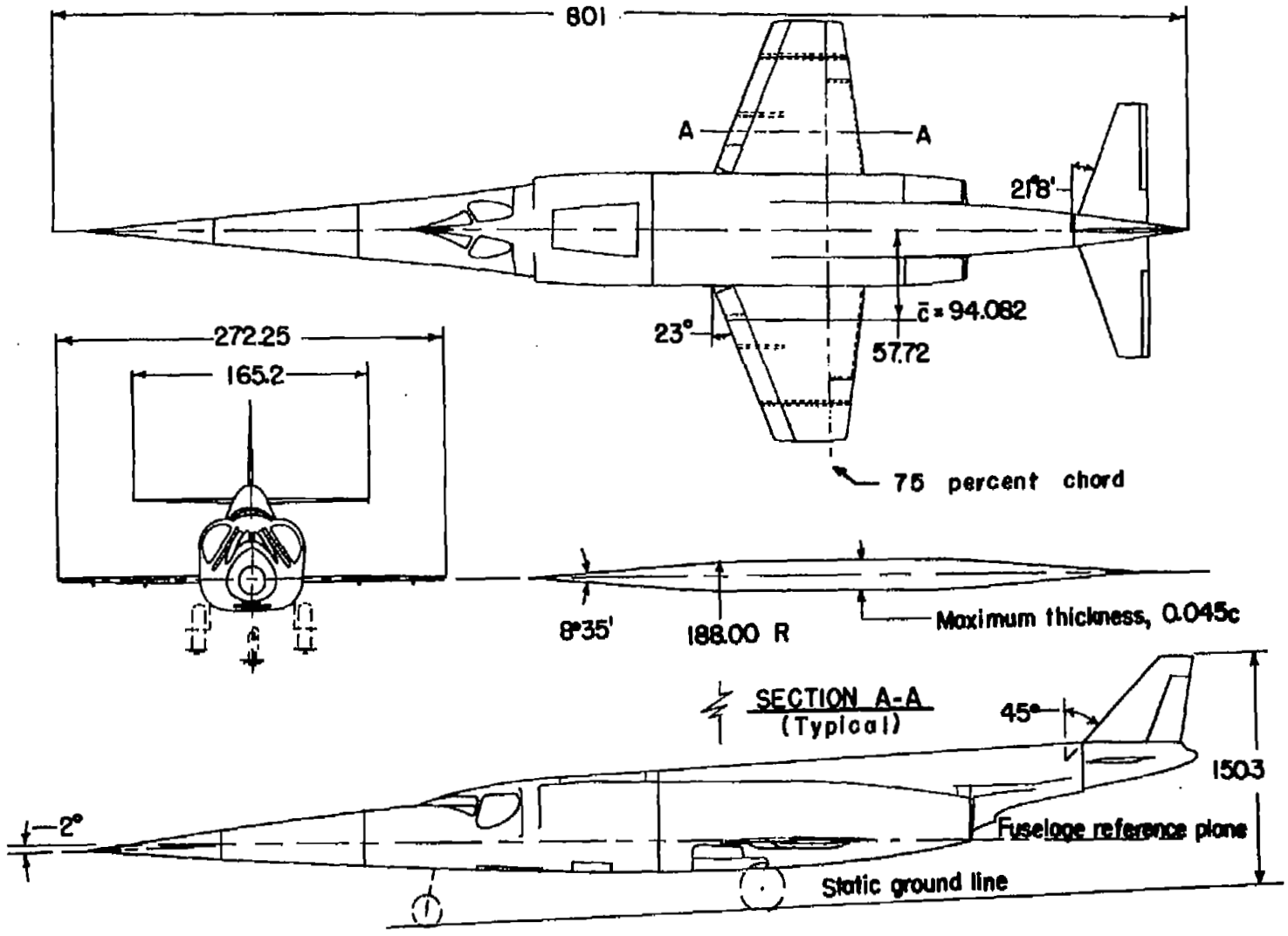

Figure 3.- Three-view drawing of X-3 airplane. All linear dimensions in inches.

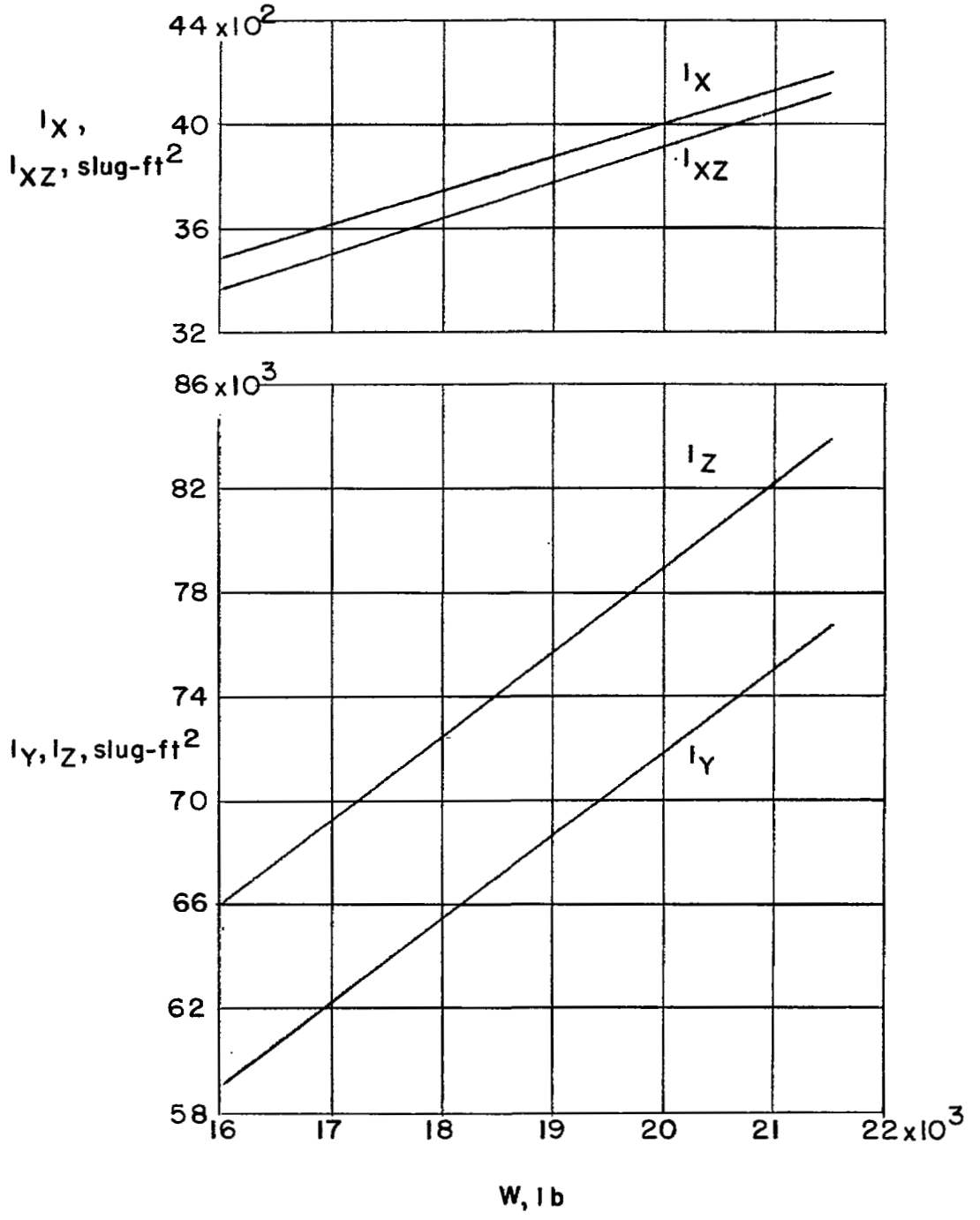

Figure 4.- Variation with airplane weight of the moment of inertia about the body axes (based on manufacturer's estimates).

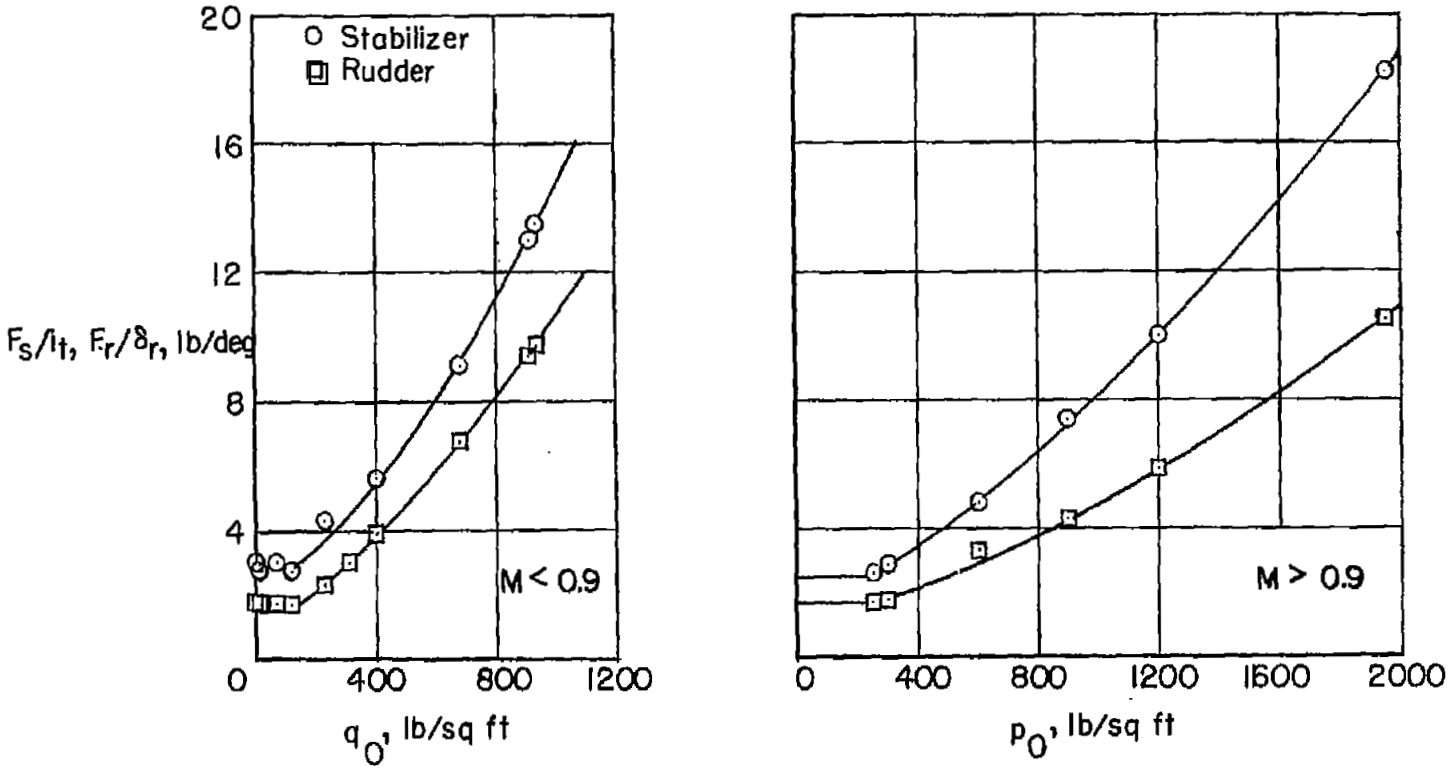

(a) Longitudinal and directional load-feel characteristics.

Figure 5.- Synthetic control-force chracteristics of the Douglas X-3 airplane obtained during ground tests.

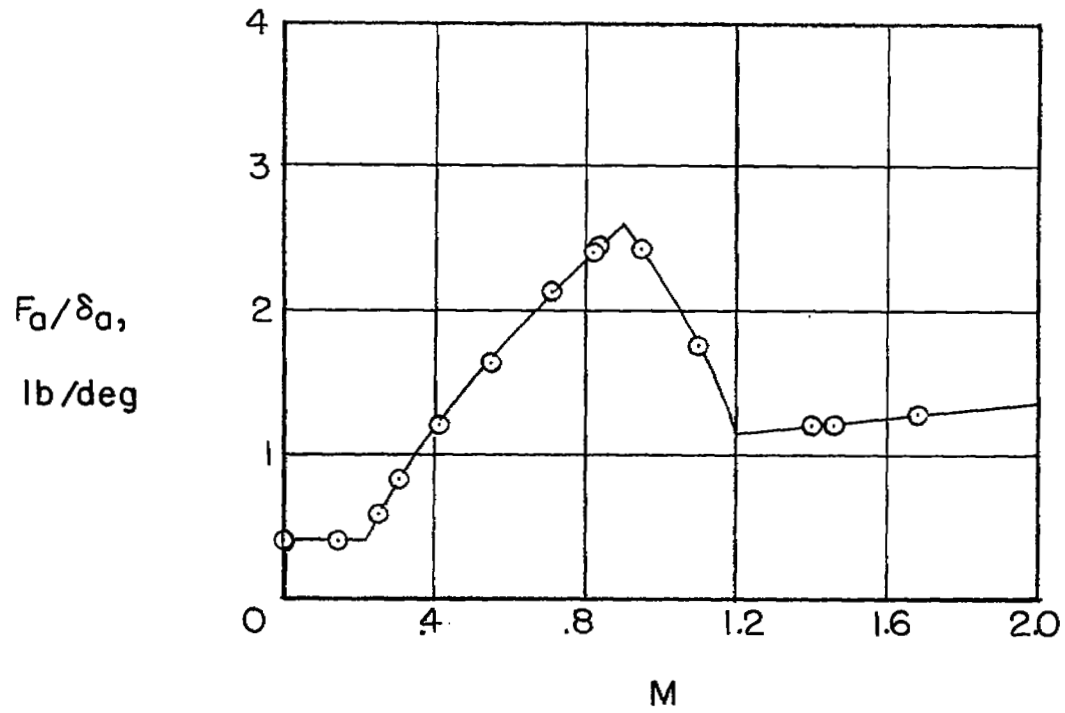

(b) Lateral load-feel characteristics.

Figure 5.- Continued.

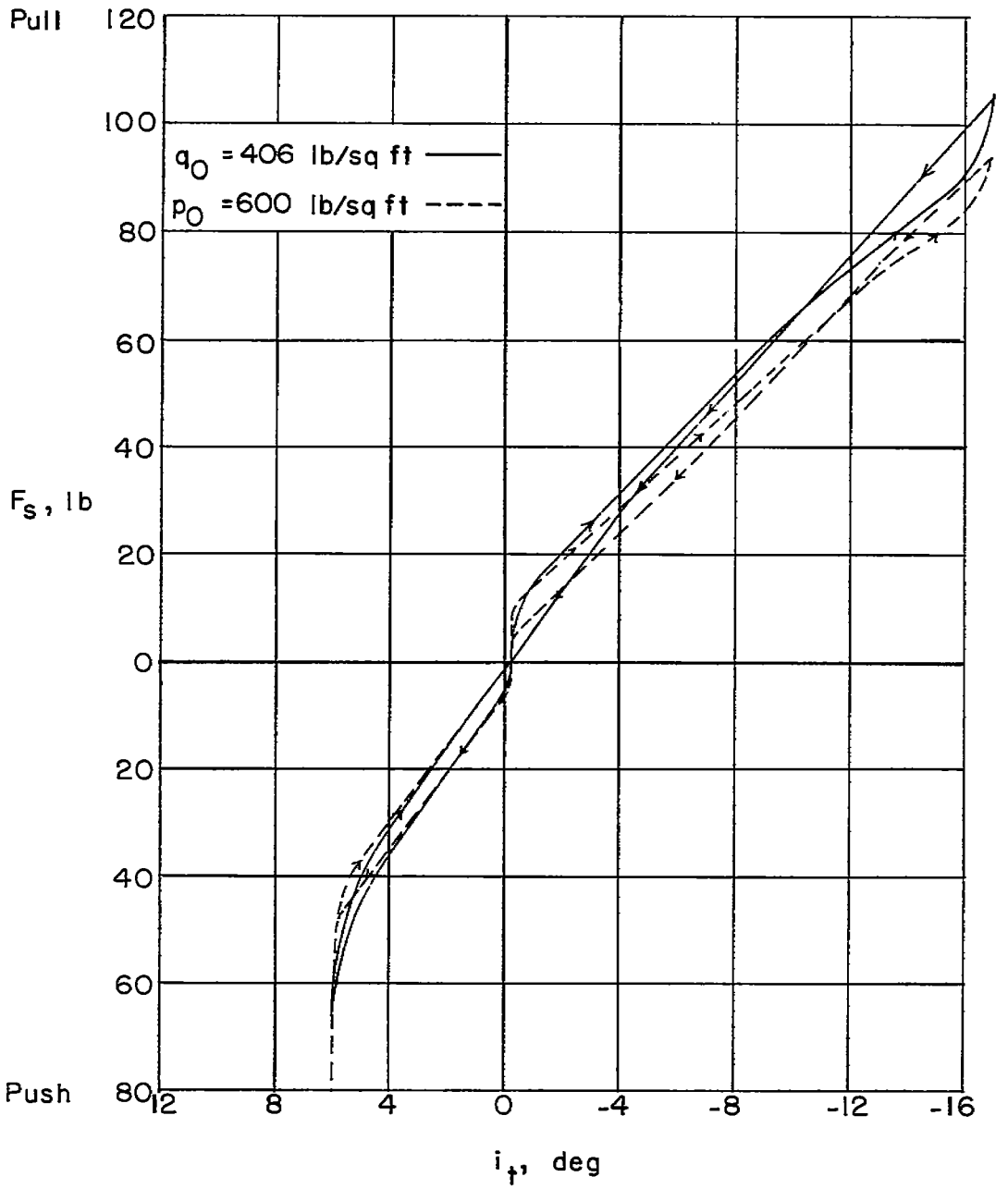

(c) Typical variations of longitudinal control force with stabilizer position.

Figure 5.- Concluded.

[redacted]

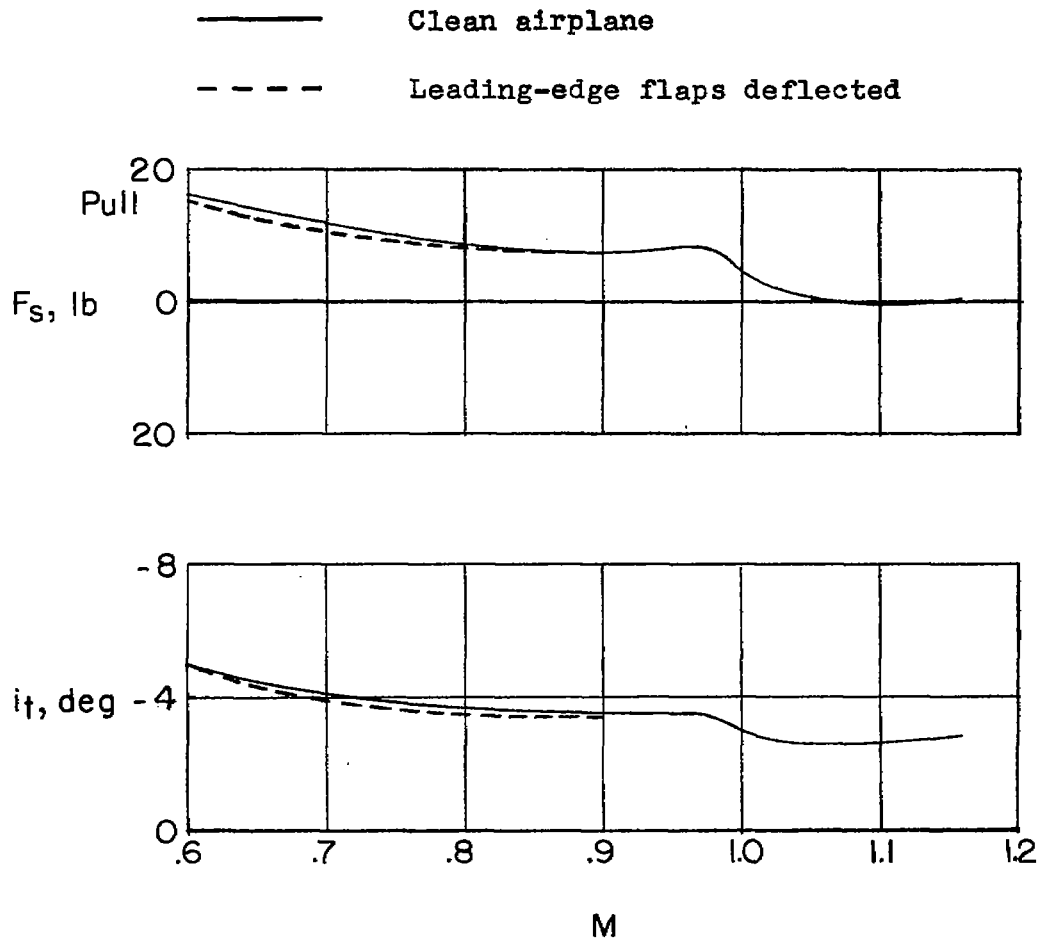

Figure 6.- Variation with Mach number of longitudinal trim characteristics for 1g flight. All data corrected to flight at h_p = 30,000 feet for W/S = 116 lb/sq ft. Douglas X-3 research airplane.

[redacted]

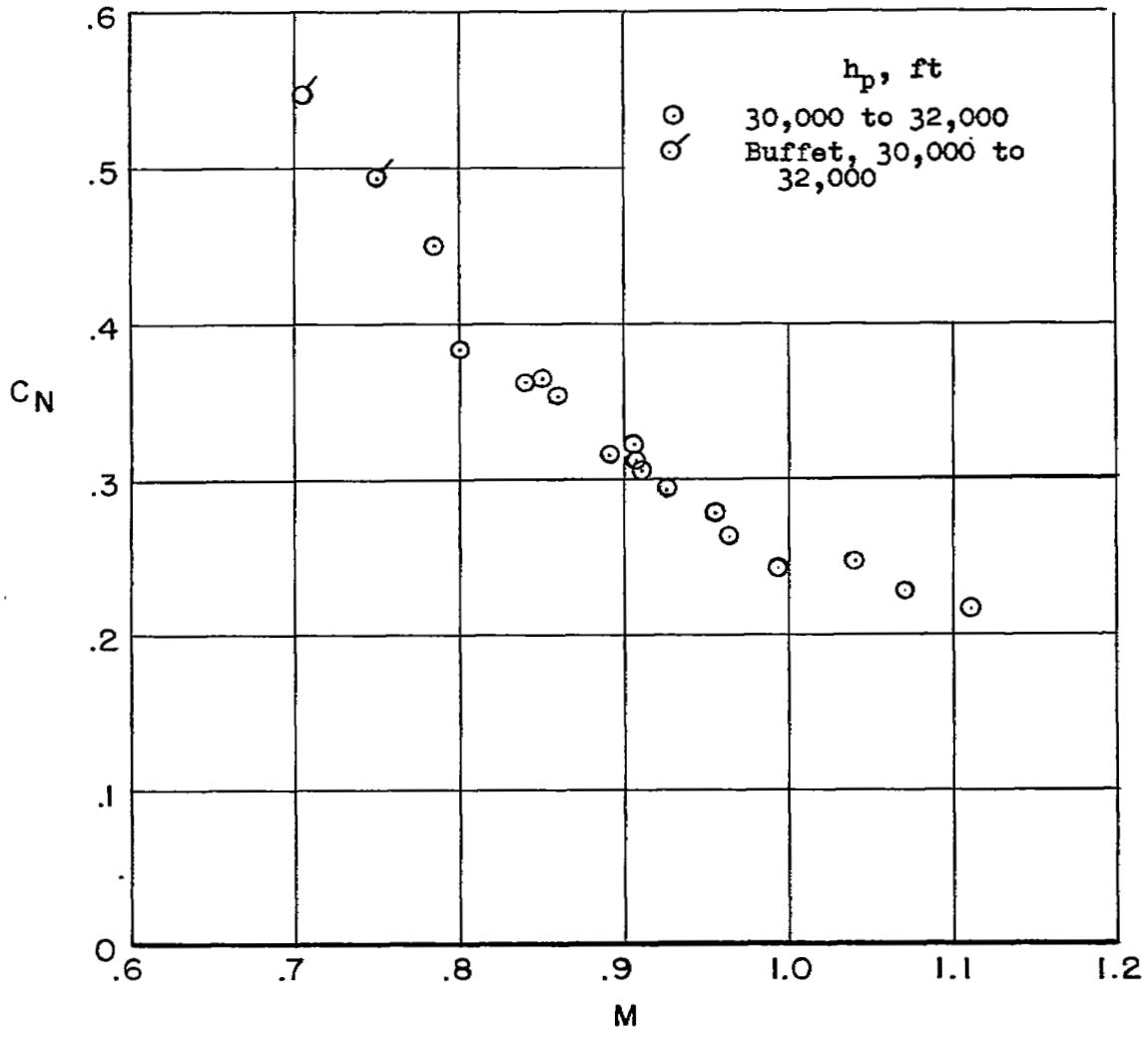

Figure 7.- Variation of normal-force coefficient with Mach number for the 1 g flight conditions at which longitudinal pulses were performed.

[redacted]

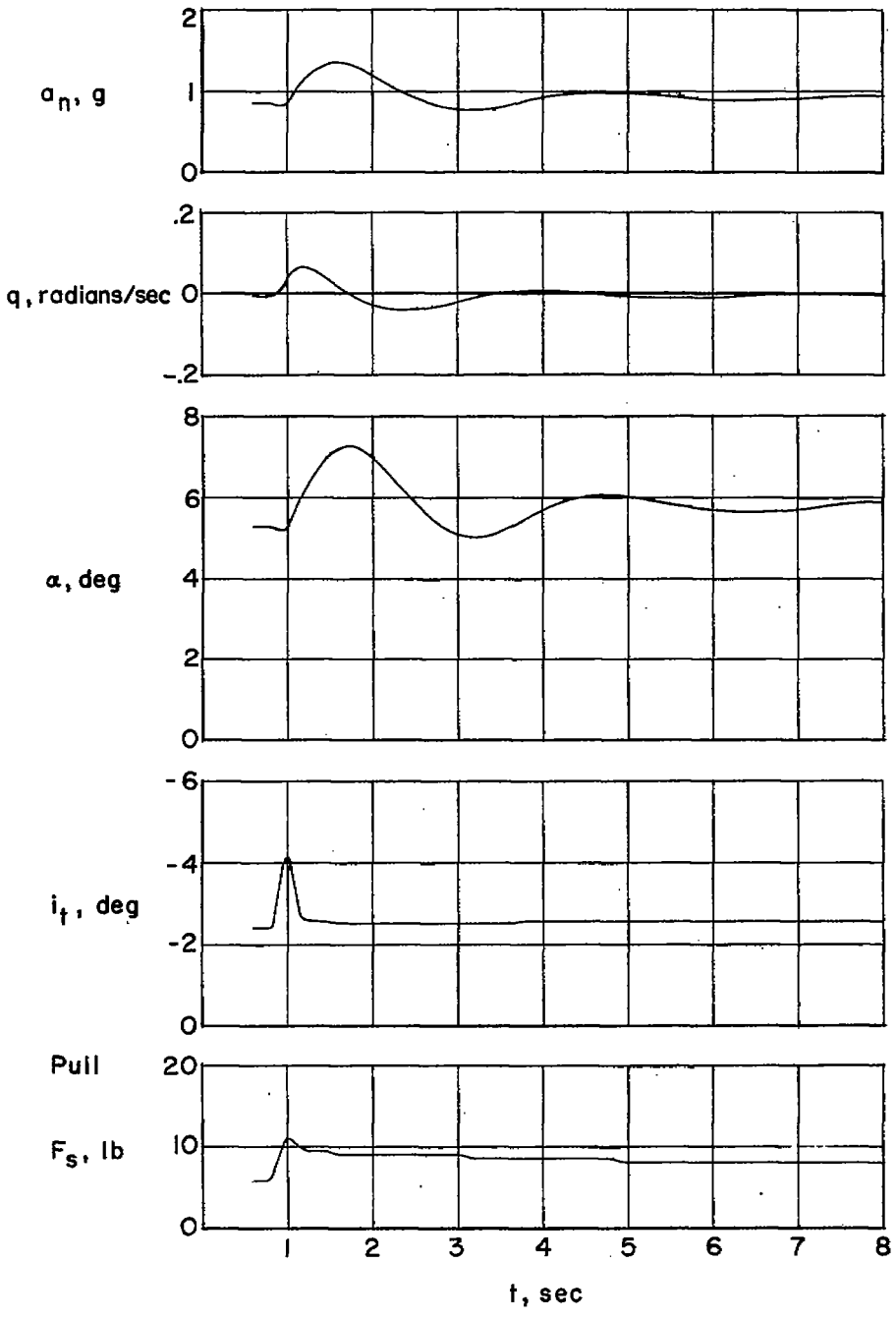

(a) $M \approx 0.84$; $h_p \approx 30{,}000$ feet.

Figure 8.- Time histories of abrupt stabilizer-pulse maneuvers.

[redacted]

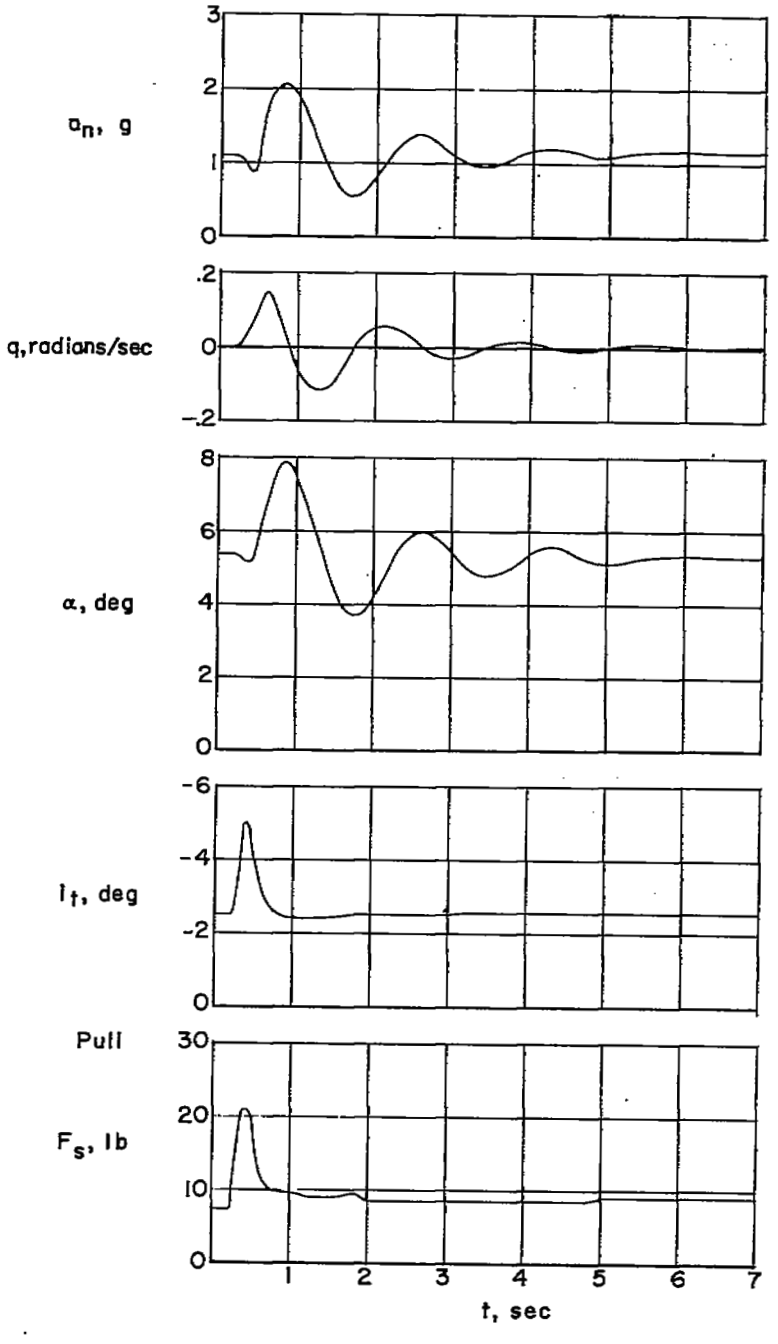

(b) $M \approx 1.04$; $h_p \approx 30{,}400$ feet.

Figure 8.- Concluded.

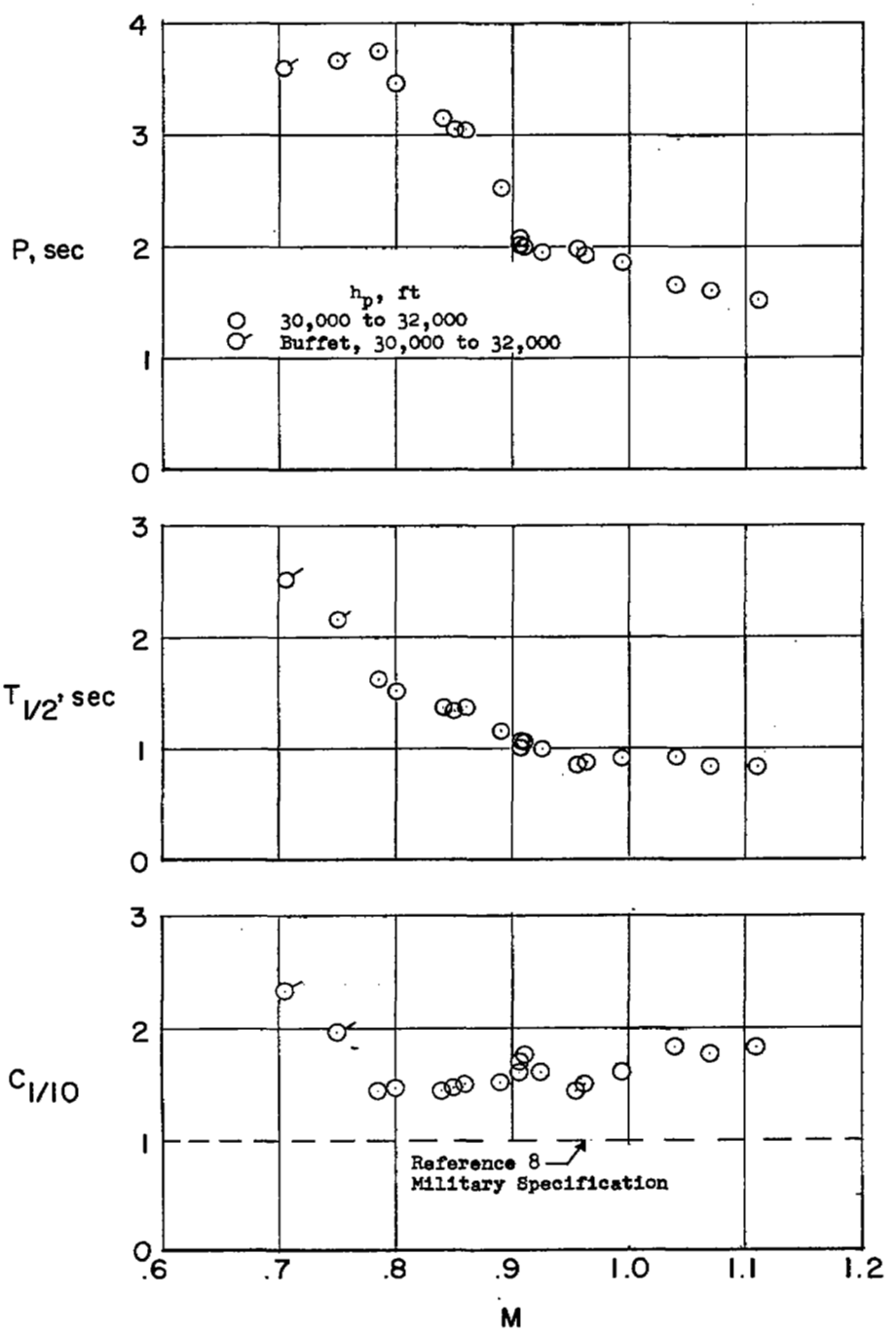

Figure 9.- Characteristics of the longitudinal oscillations following abrupt stabilizer pulses as a function of Mach number.

[redacted]

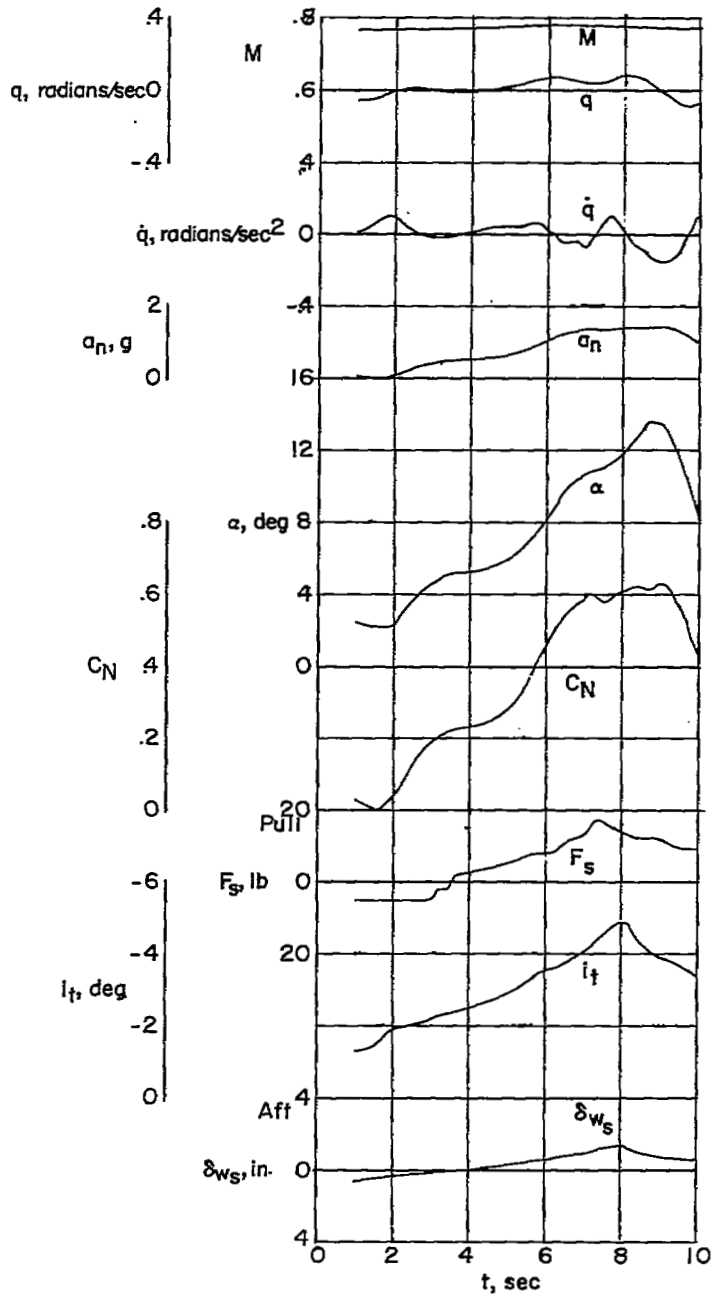

(a) $h_p \approx 32{,}500$ feet; $\delta_{f_{le}} = 0°$.

Figure 10.- Time histories of accelerated longitudinal maneuvers for the Douglas X-3 research airplane.

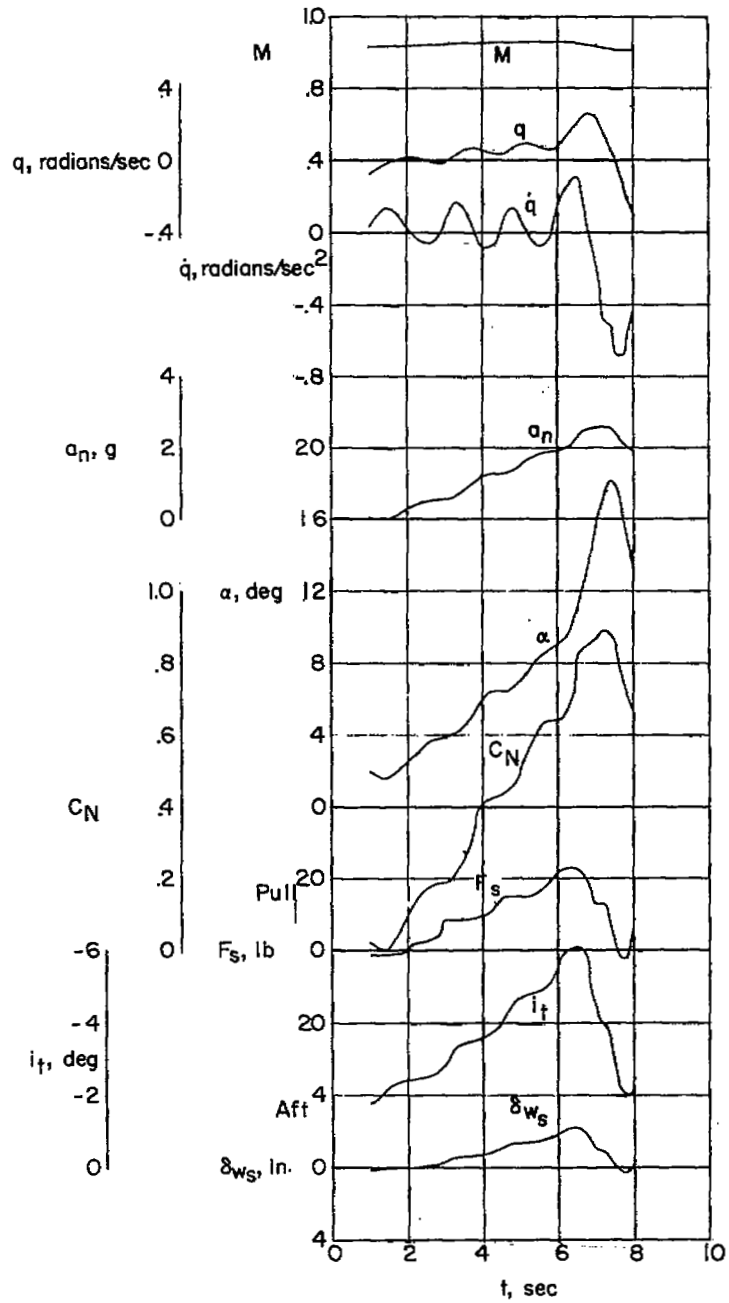

(b) $h_p \approx 33{,}500$ feet; $\delta_{f_{le}} = 0^\circ$.

Figure 10.- Continued.

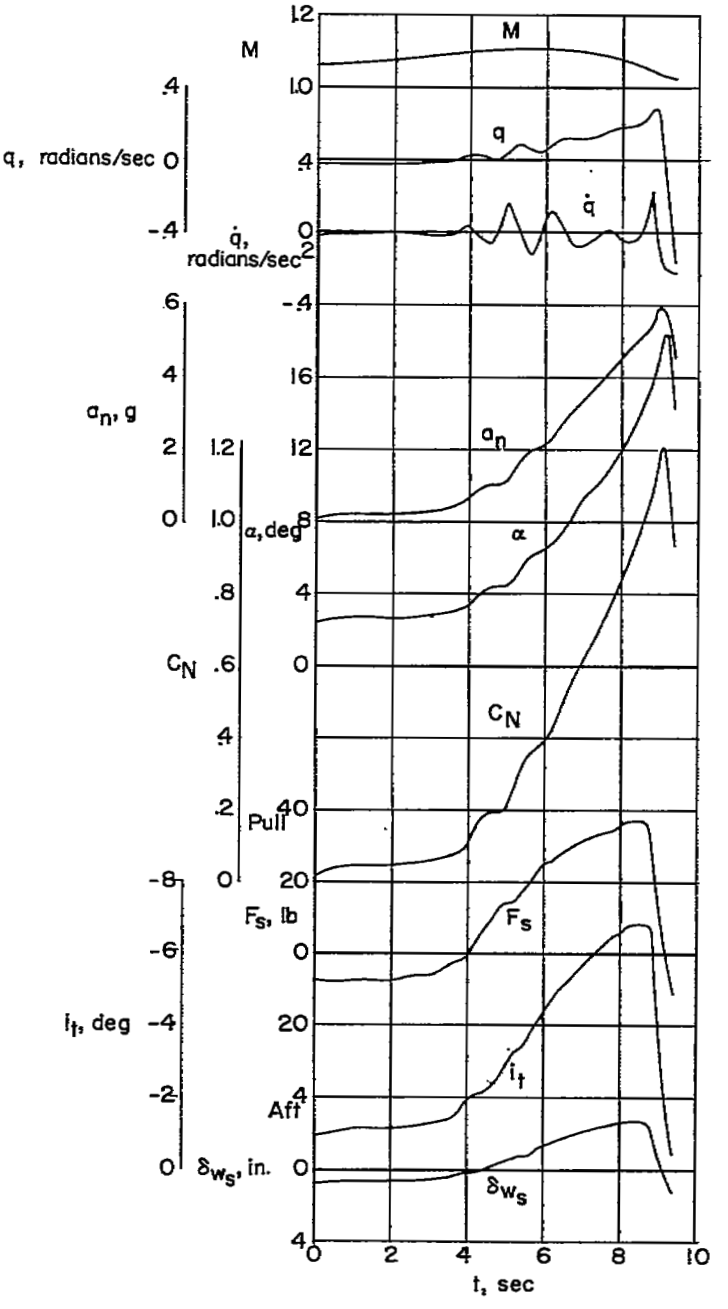

(c) $h_p \approx 28{,}000$ feet; $\delta_{f_{le}} = 0^\circ$.

Figure 10.- Continued.

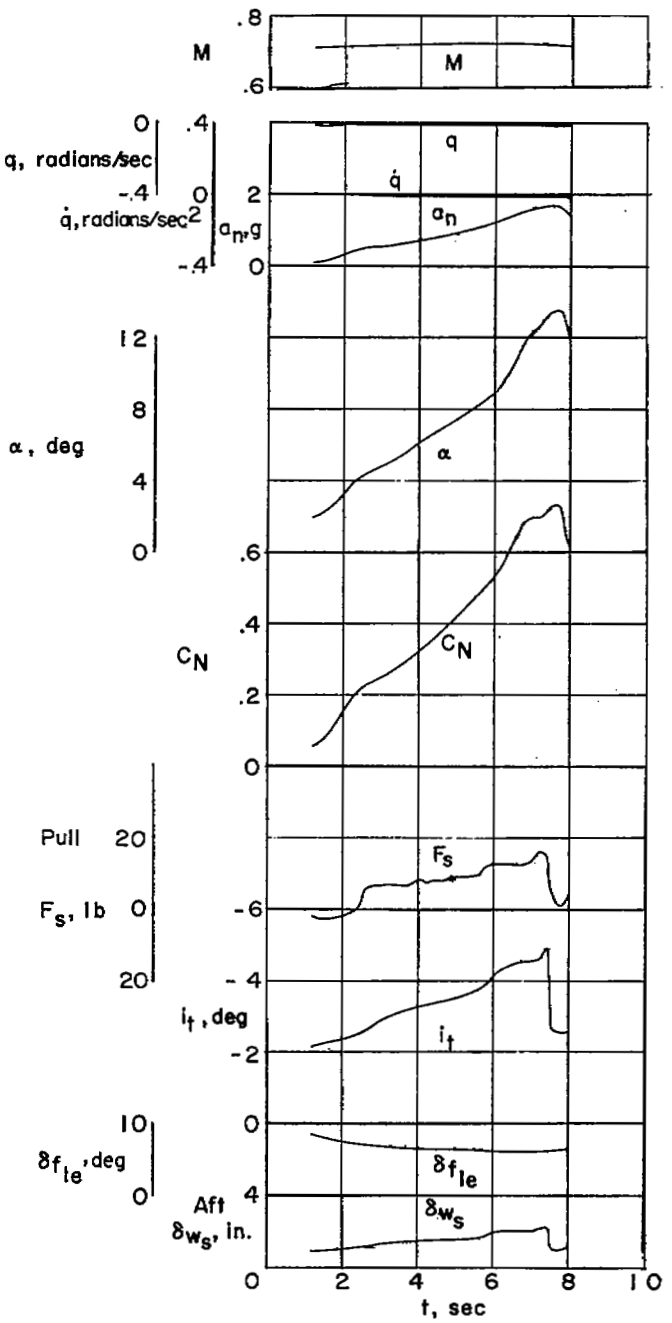

(d) $h_p \approx 28{,}500$ feet.

Figure 10.- Continued.

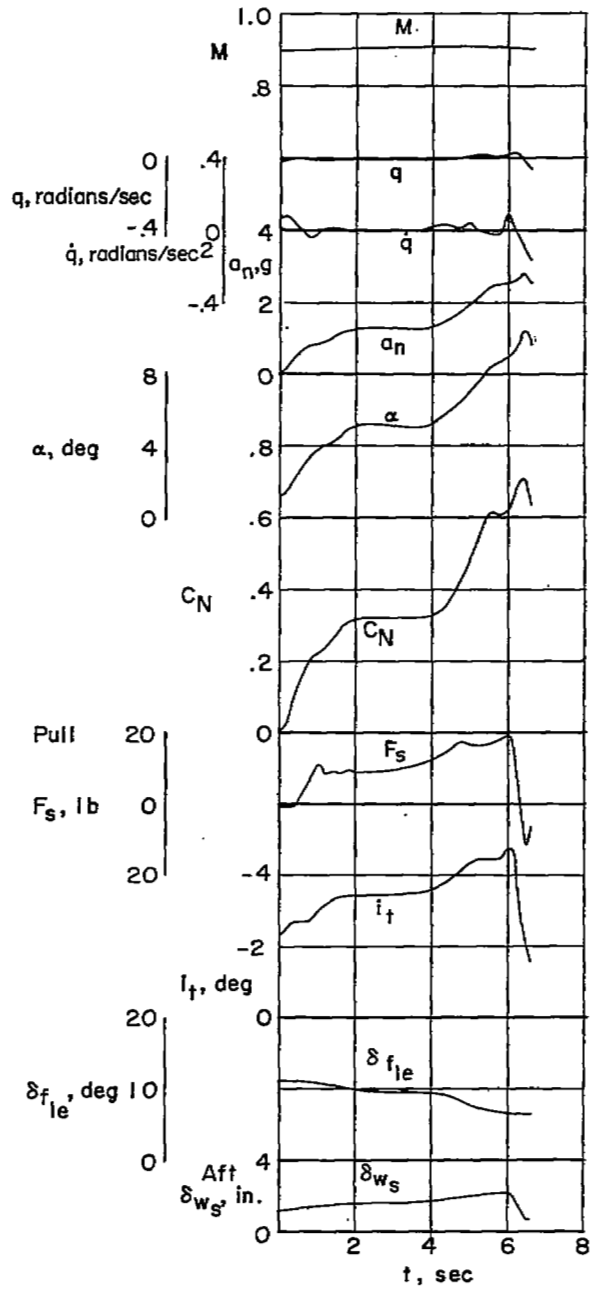

(e) $h_p \approx 25{,}500$ feet.

Figure 10.- Concluded.

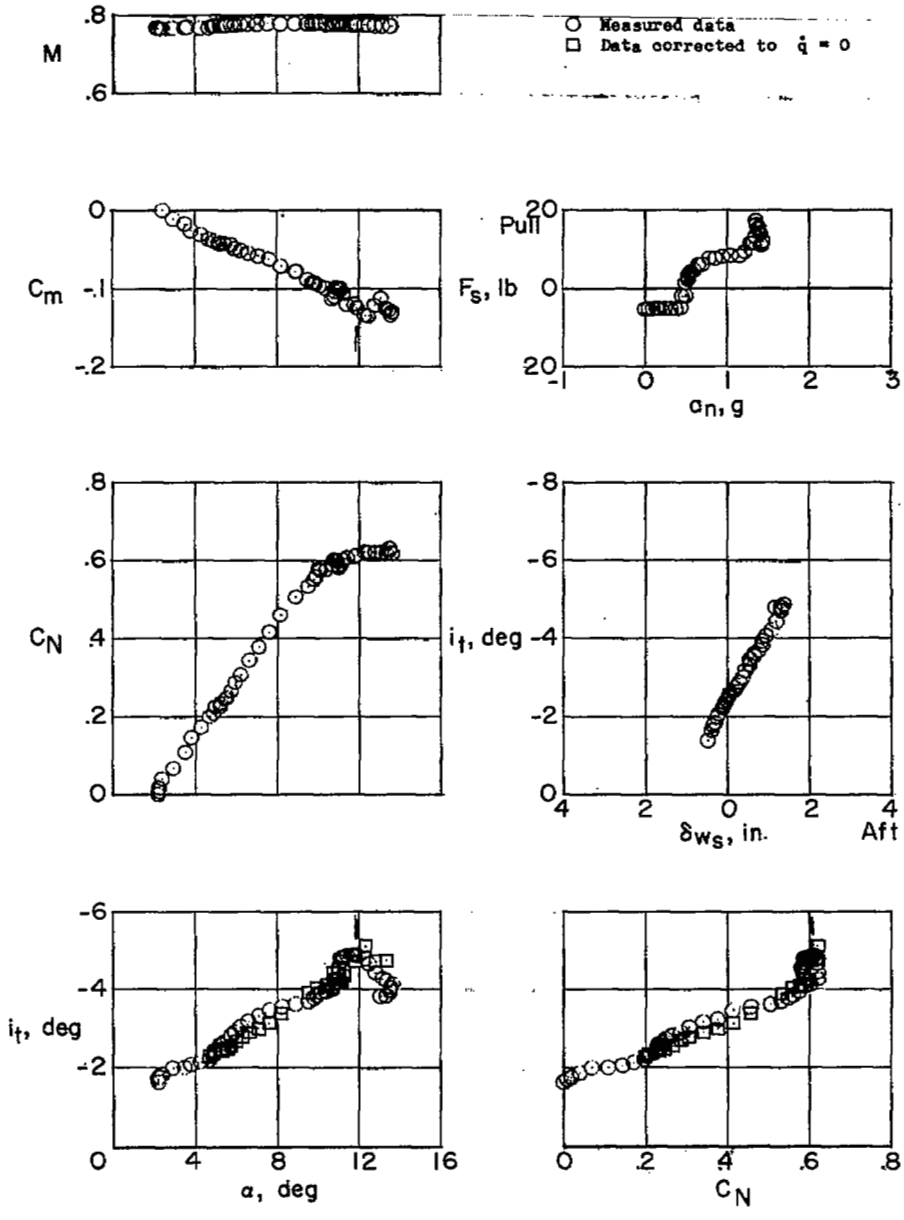

(a) $h_p \approx 32{,}500$ feet; $\delta_{f_{le}} = 0^\circ$.

Figure 11.- Static longitudinal stability characteristics of the Douglas X-3 research airplane in accelerated flight.

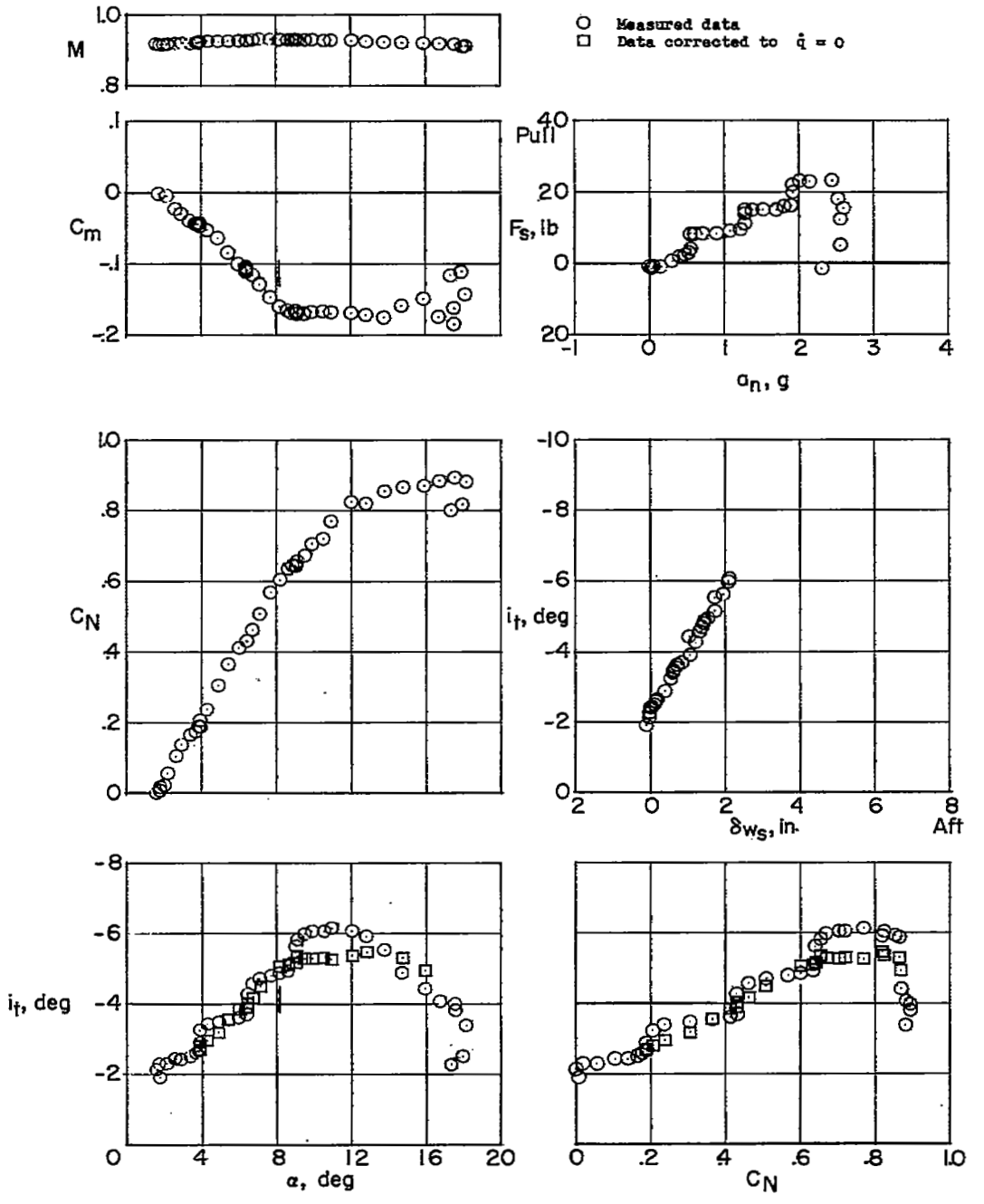

(b) $h_p \approx 33{,}500$ feet; $\delta_{f_{le}} = 0^\circ$.

Figure 11.- Continued.

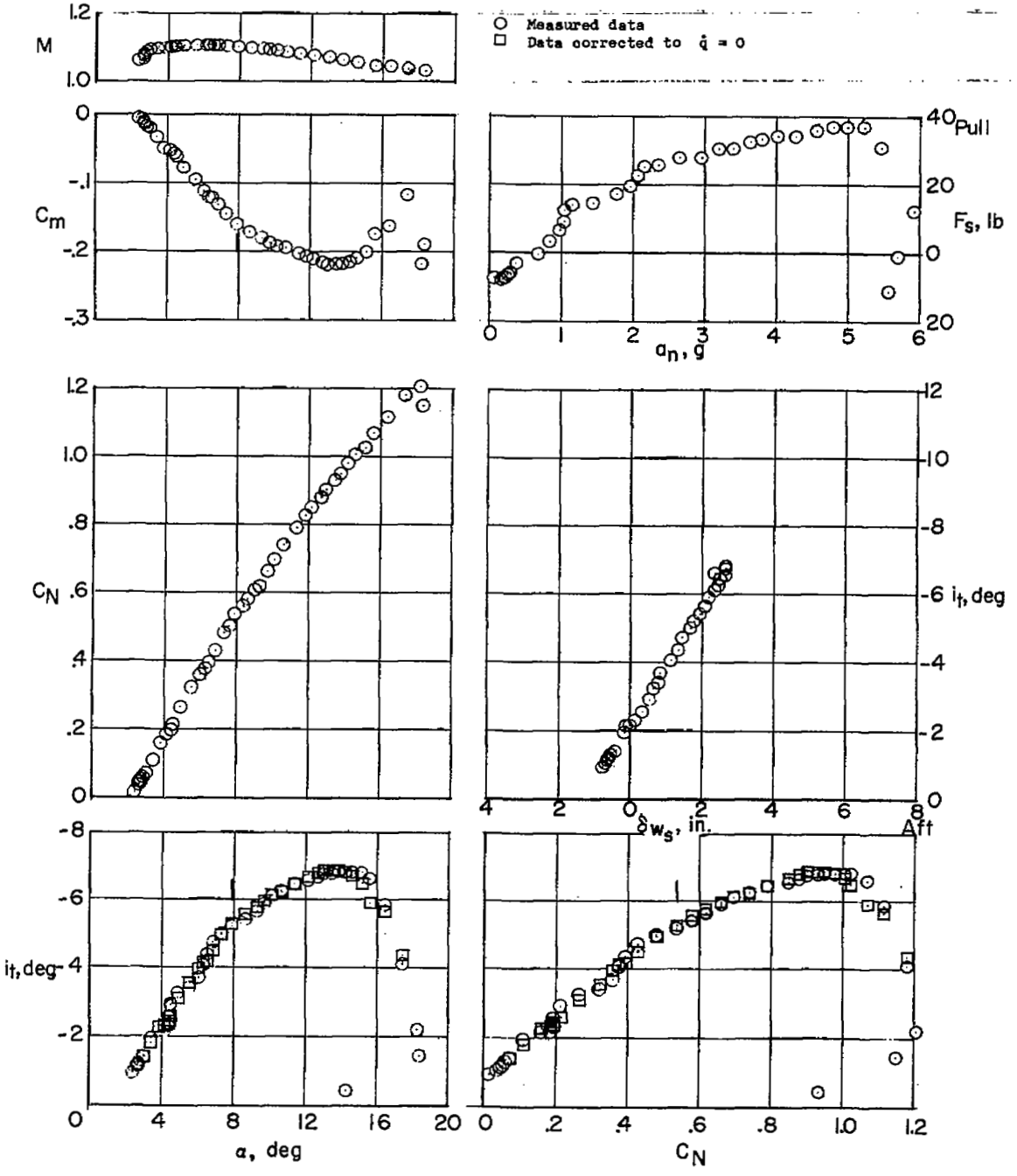

(c) $h_p \approx 28{,}000$ feet; $\delta_{f_{le}} = 0°$.

Figure 11.- Continued.

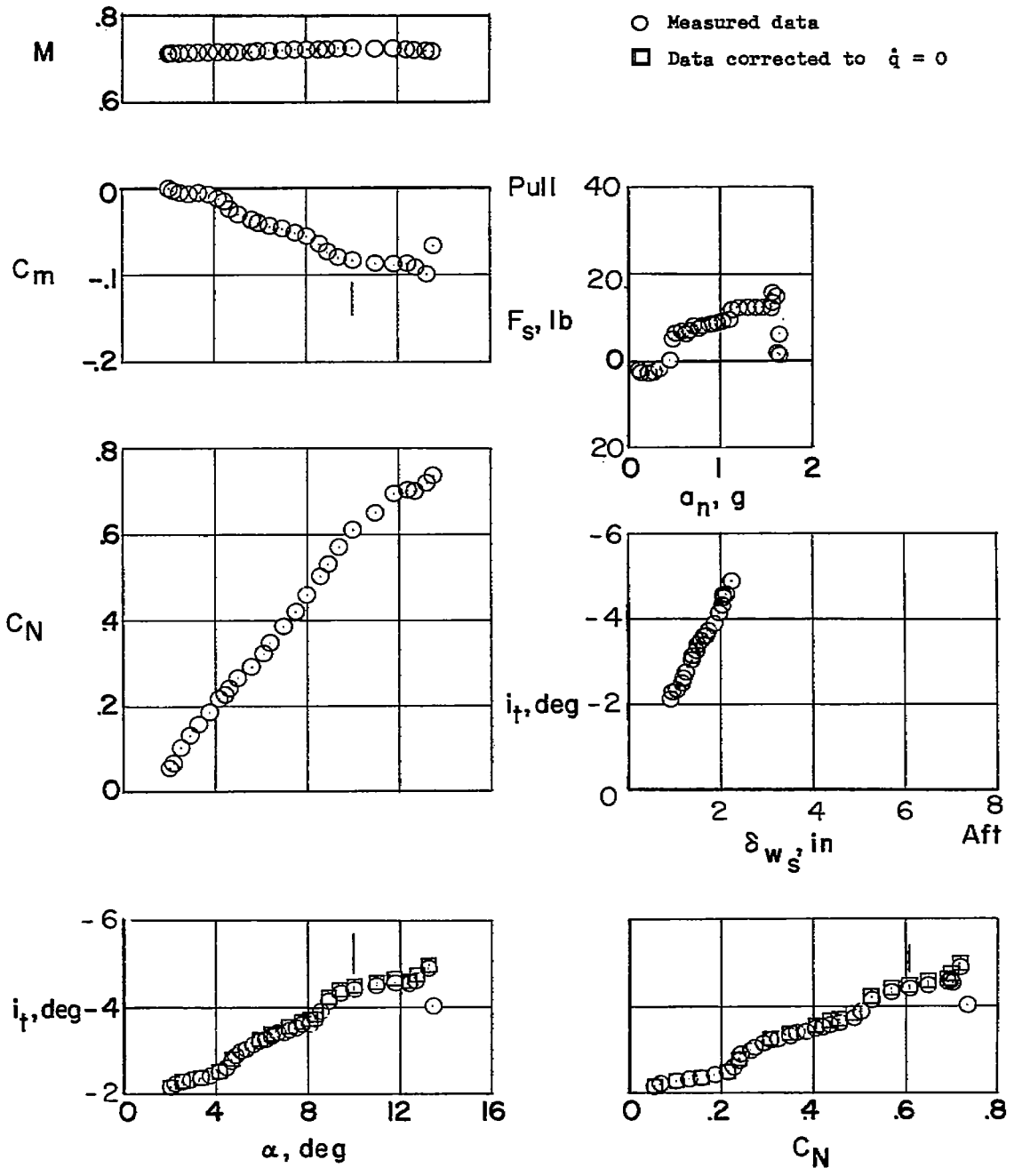

(d) $h_p \approx 28{,}500$ feet; $\delta_{f_{le}} \approx 7^\circ$.

Figure 11.- Continued.

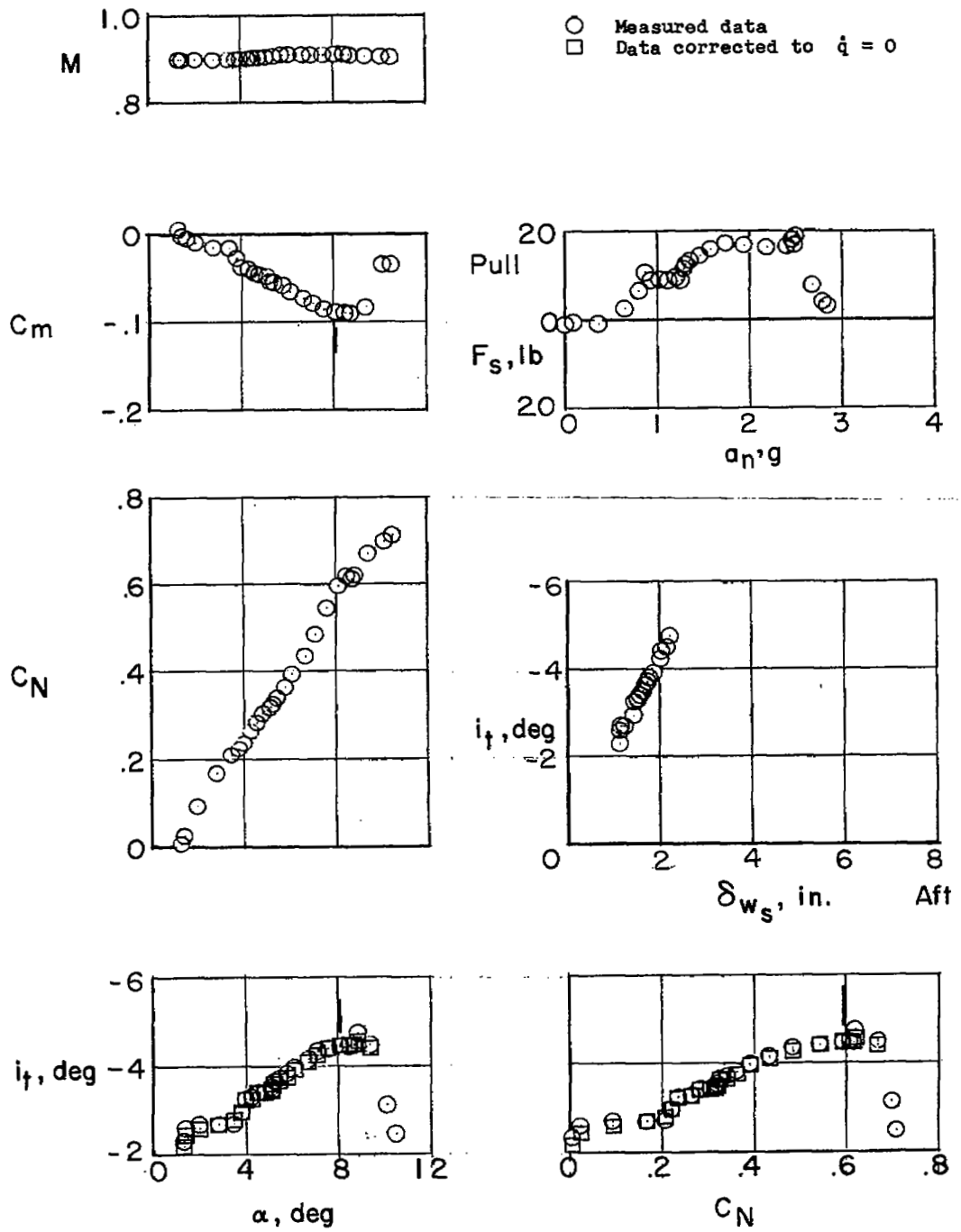

(e) $h_p \approx 25{,}500$ feet; $\delta_{f_{le}} \approx 8°$.

Figure 11.- Concluded.

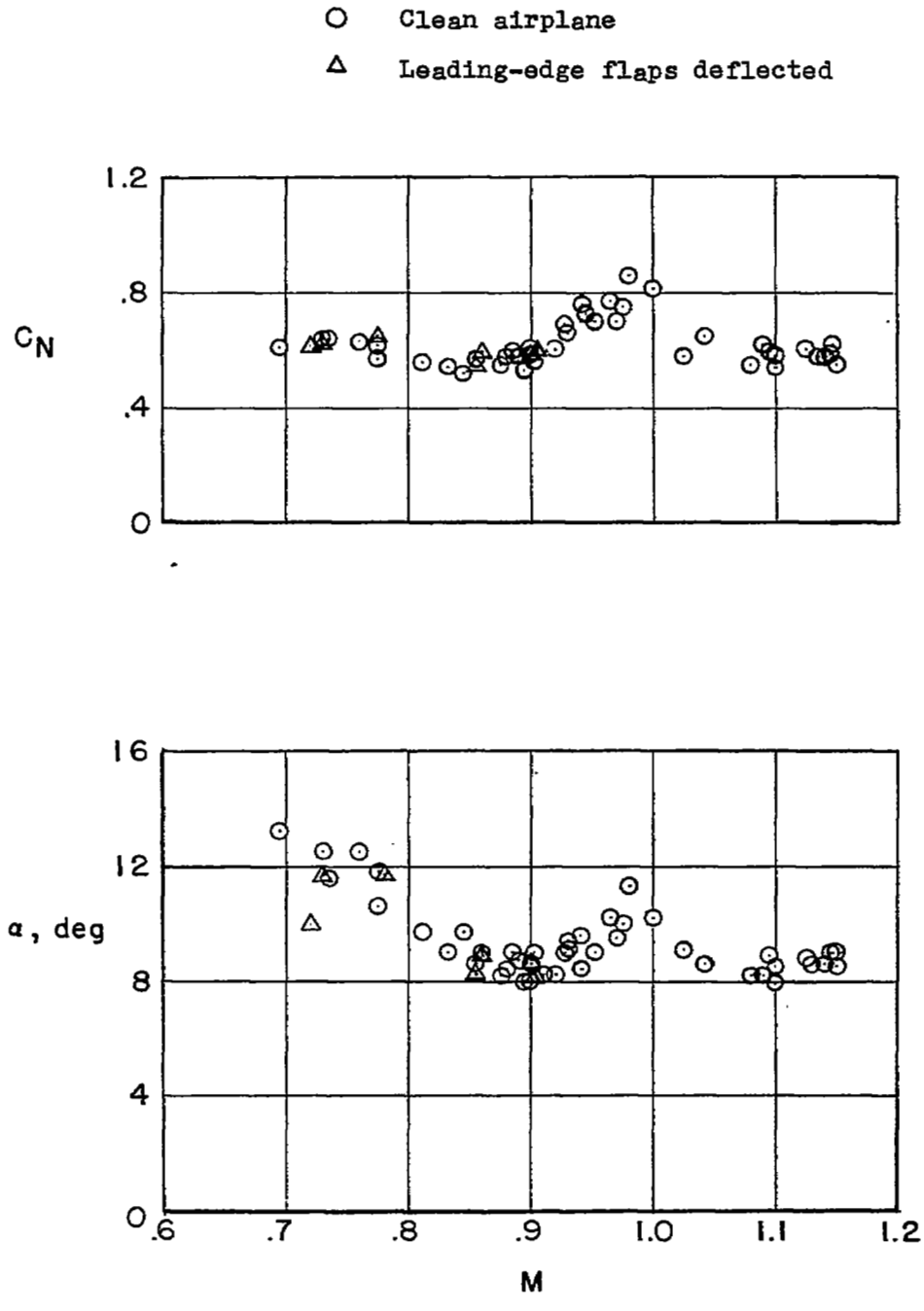

Figure 12.- Variation with Mach number of normal-force coefficient and angle of attack for the decay in stick-fixed longitudinal stability of the Douglas X-3 research airplane.

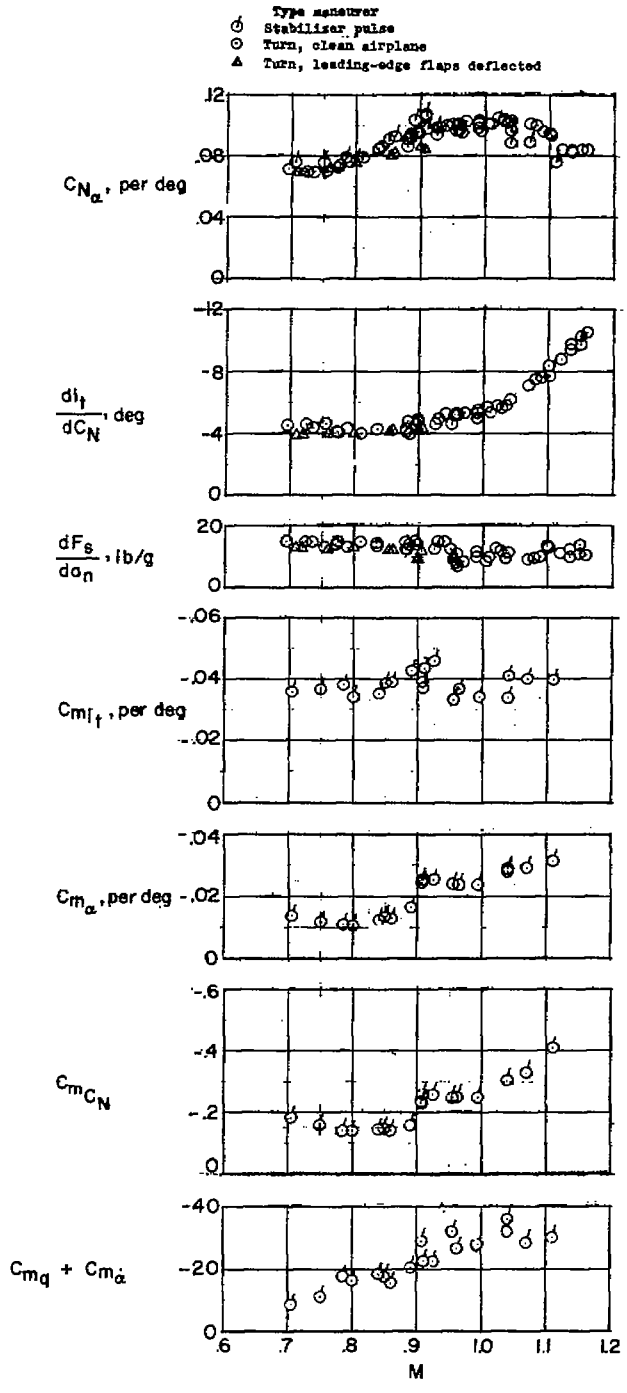

Figure 13.- Stability and control effectiveness parameters as a function of Mach number.

[redacted]

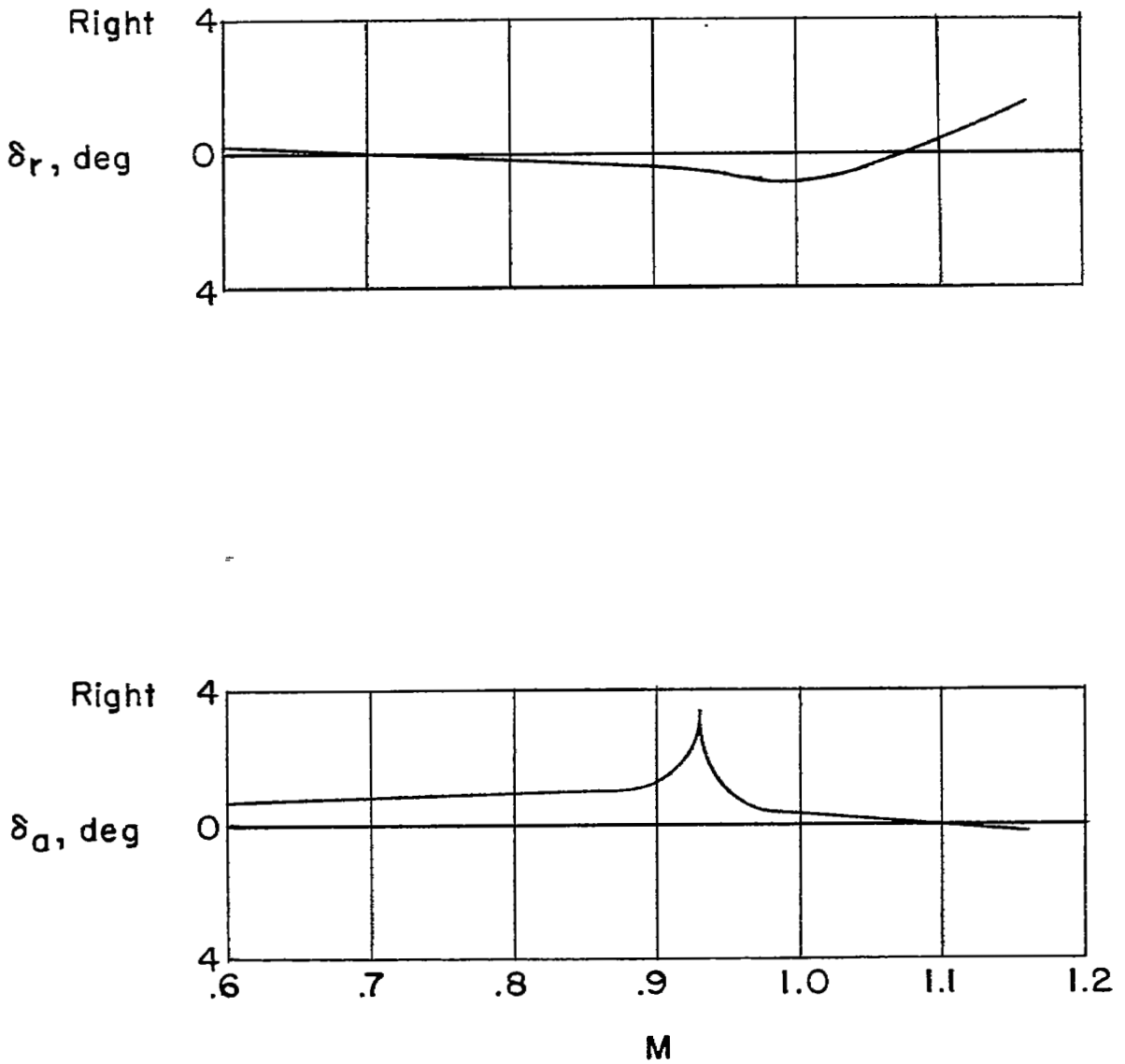

Figure 14.- Variation with Mach number of the rudder and aileron positions required to trim the airplane in 1 g flight at $h_p \approx 30{,}000$ feet.

[redacted]

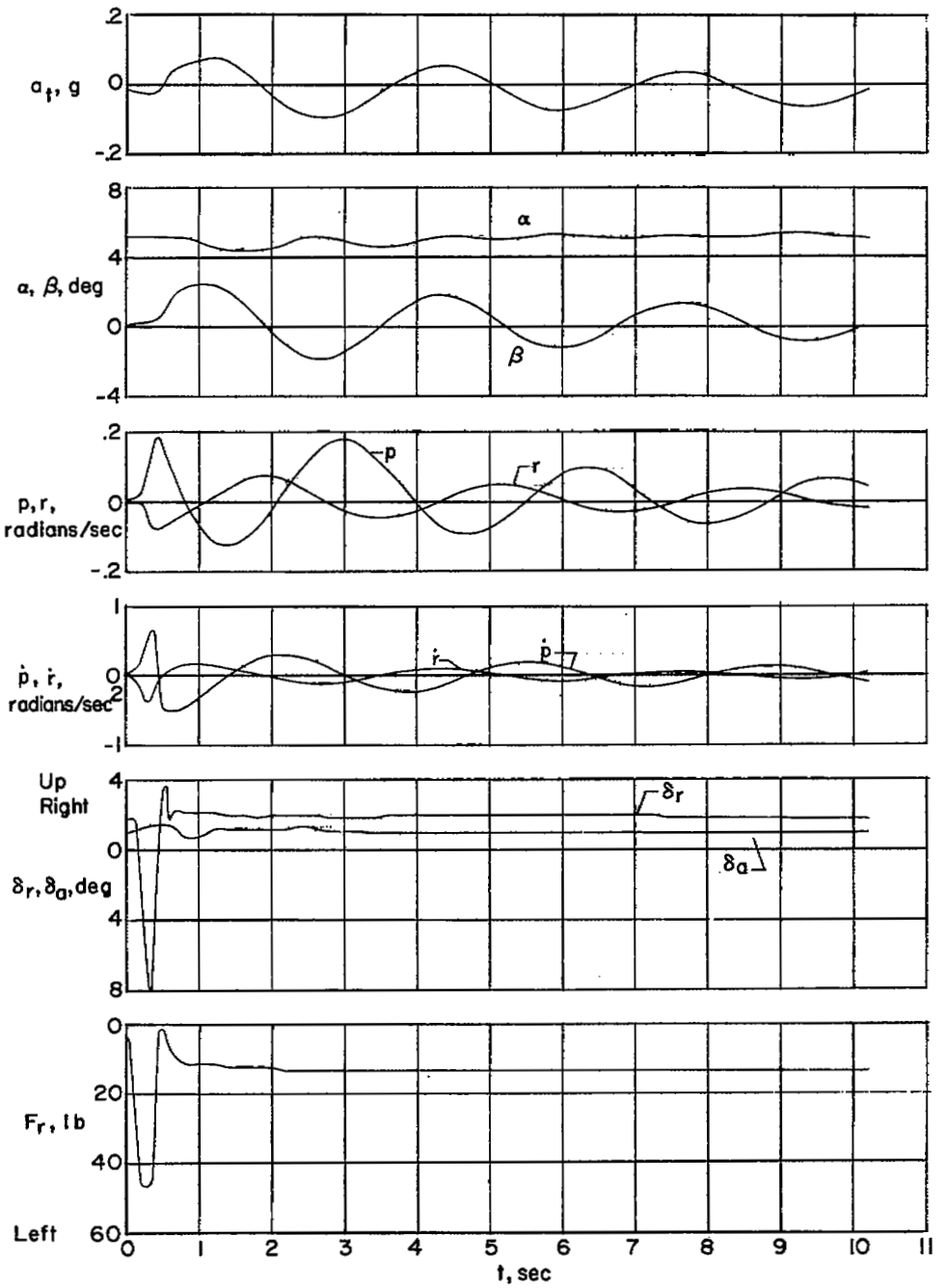

(a) $M \approx 0.95$; $h_p \approx 32{,}600$ feet.

Figure 15.- Time histories of abrupt rudder-pulse maneuvers.

[redacted]

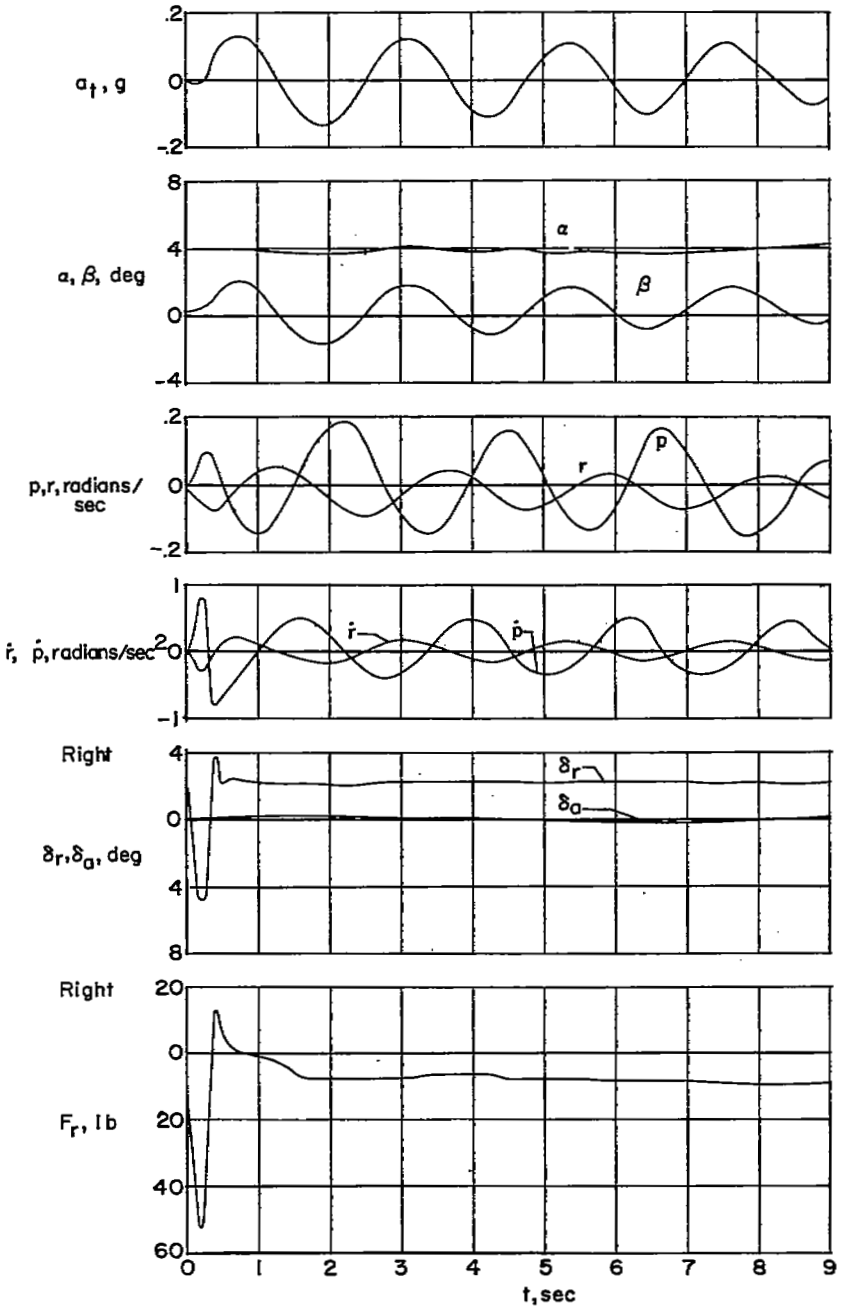

(b) $M \approx 1.11$; $h_p \approx 28{,}500$ feet.

Figure 15.- Concluded.

[redacted]

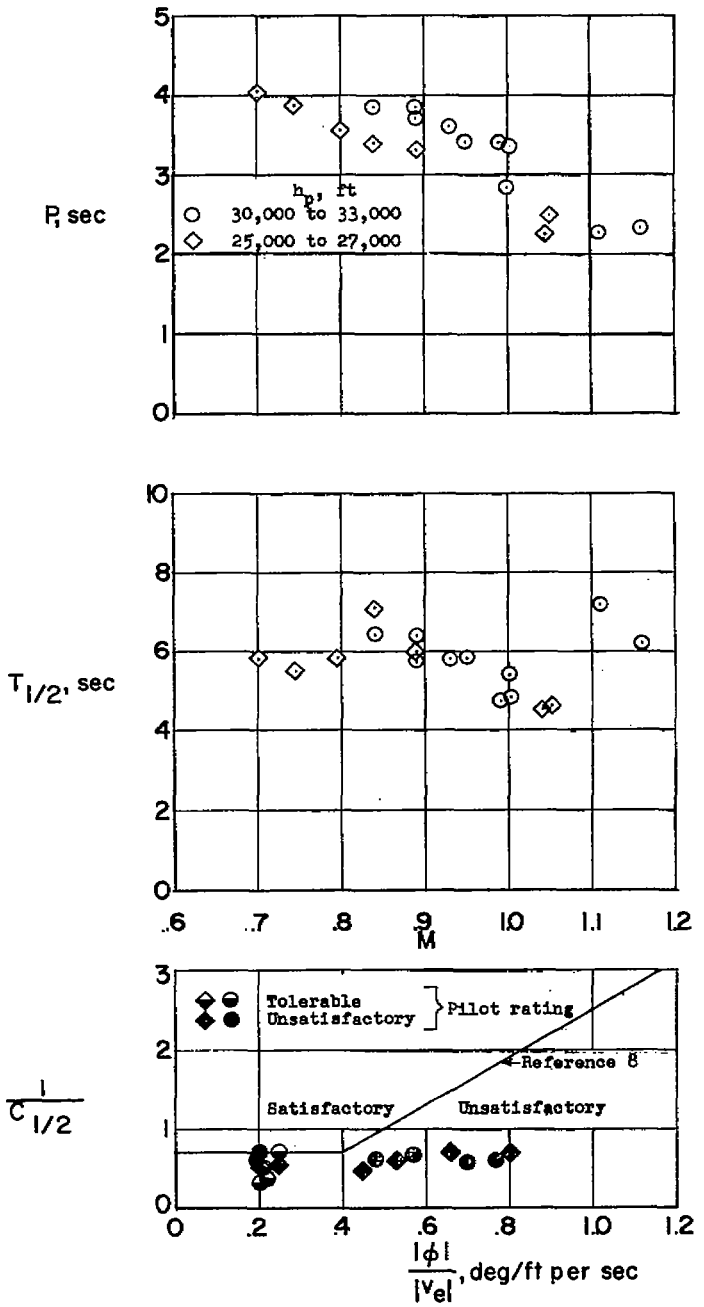

Figure 16.- Characteristics of the lateral oscillations following abrupt rudder pulses as a function of Mach number and $\frac{\varphi}{v_e}$.

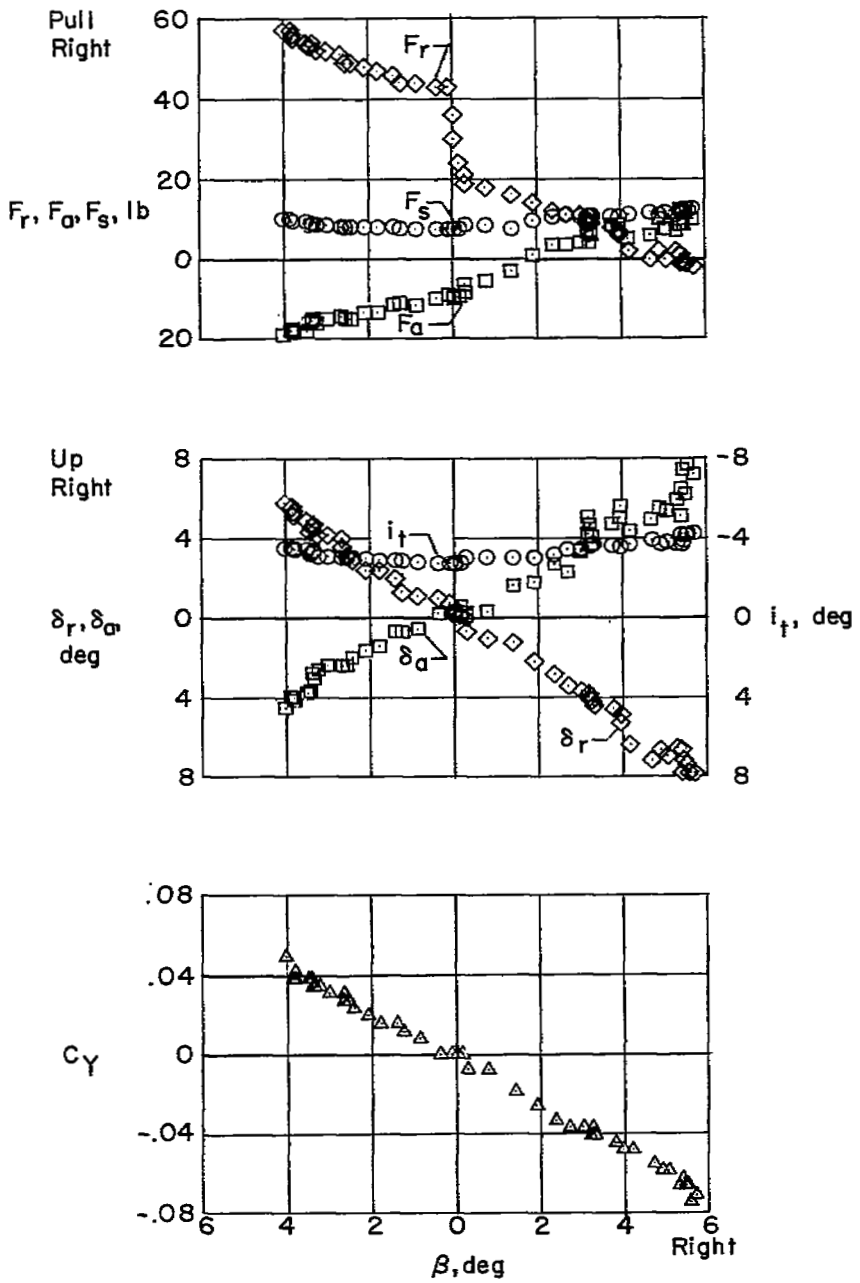

(a) $M \approx 0.76$; $h_p \approx 27{,}300$ feet.

Figure 17.- Variation of control forces, control positions, and side-force coefficient with sideslip angle during constant-heading sideslips of the Douglas X-3 research airplane.

[redacted]

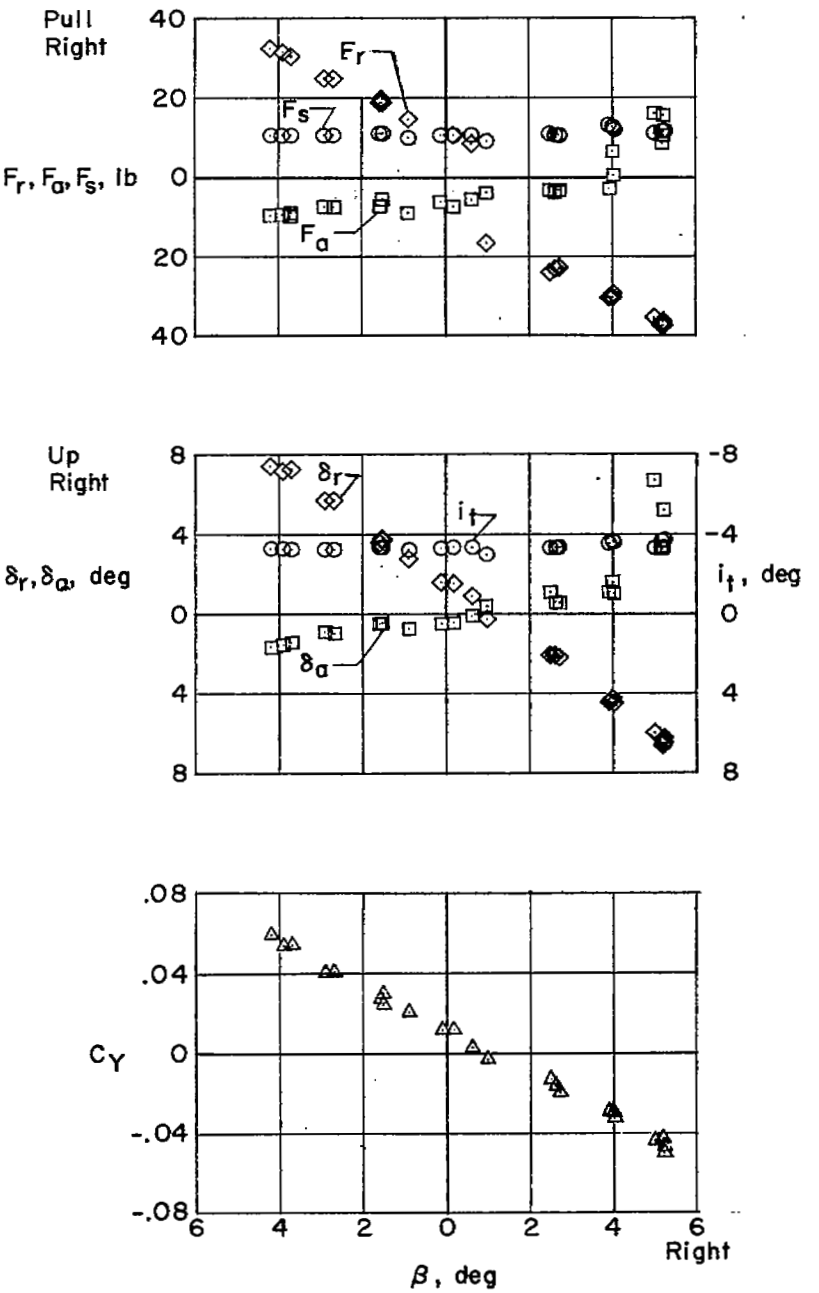

(b) $M \approx 0.95$; $h_p \approx 33{,}000$ feet.

Figure 17.- Continued.

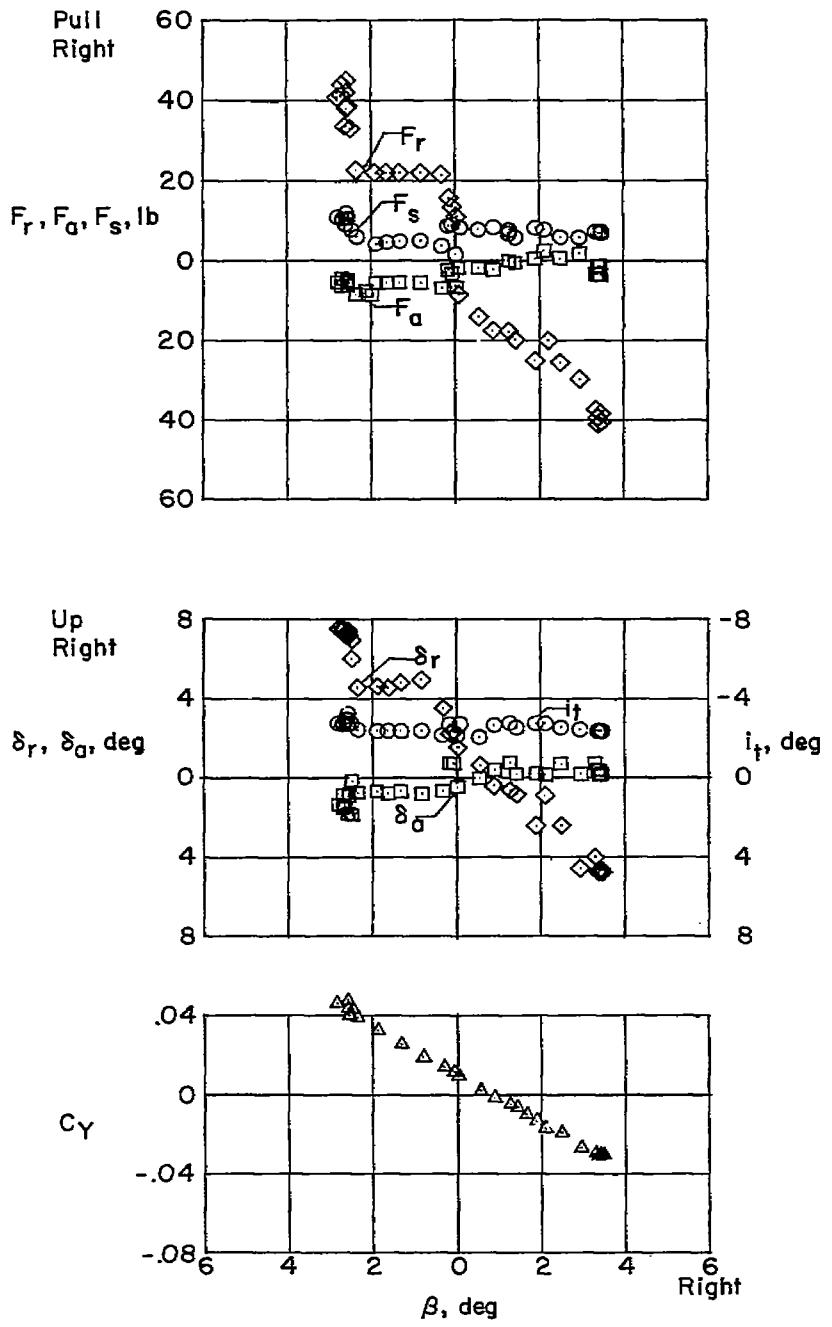

(c) $M \approx 1.09$; $h_p \approx 29{,}000$ feet.

Figure 17.- Concluded.

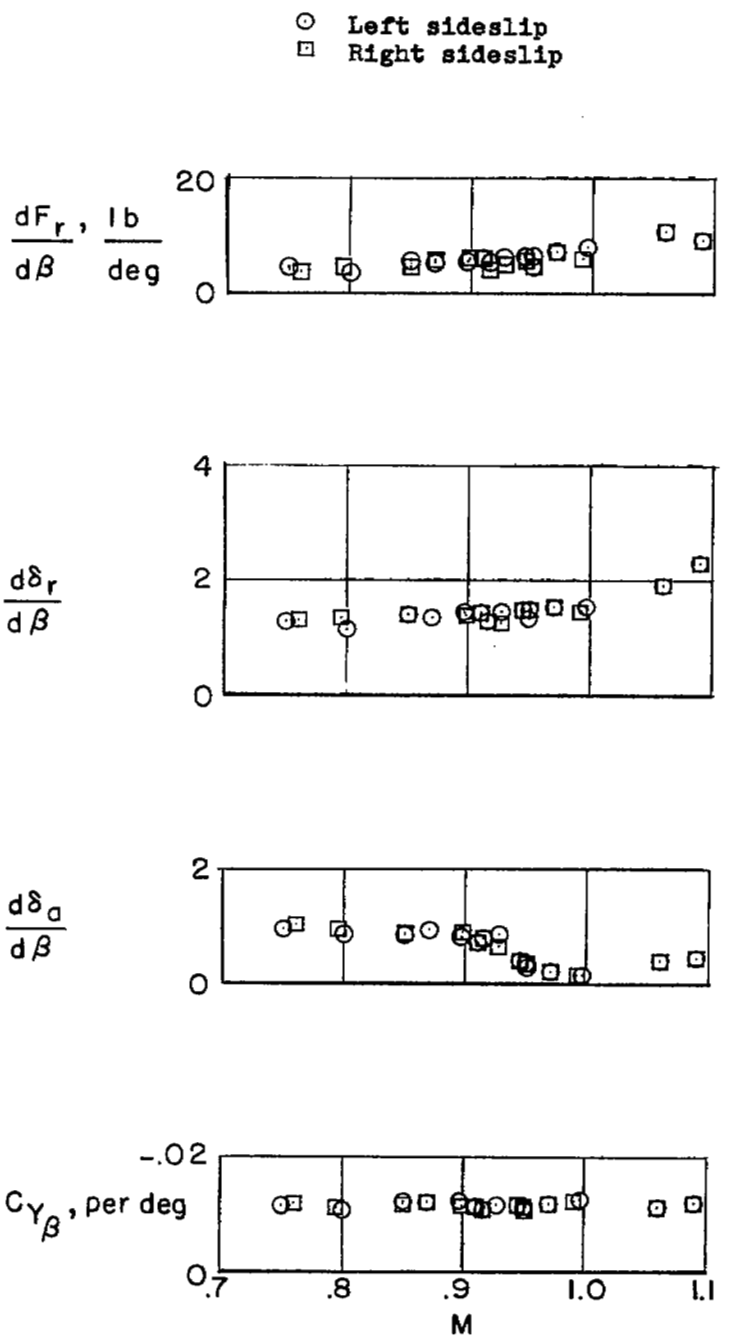

Figure 18.- Static lateral stability and control effectiveness parameters as a function of Mach number determined during constant-heading sideslips.

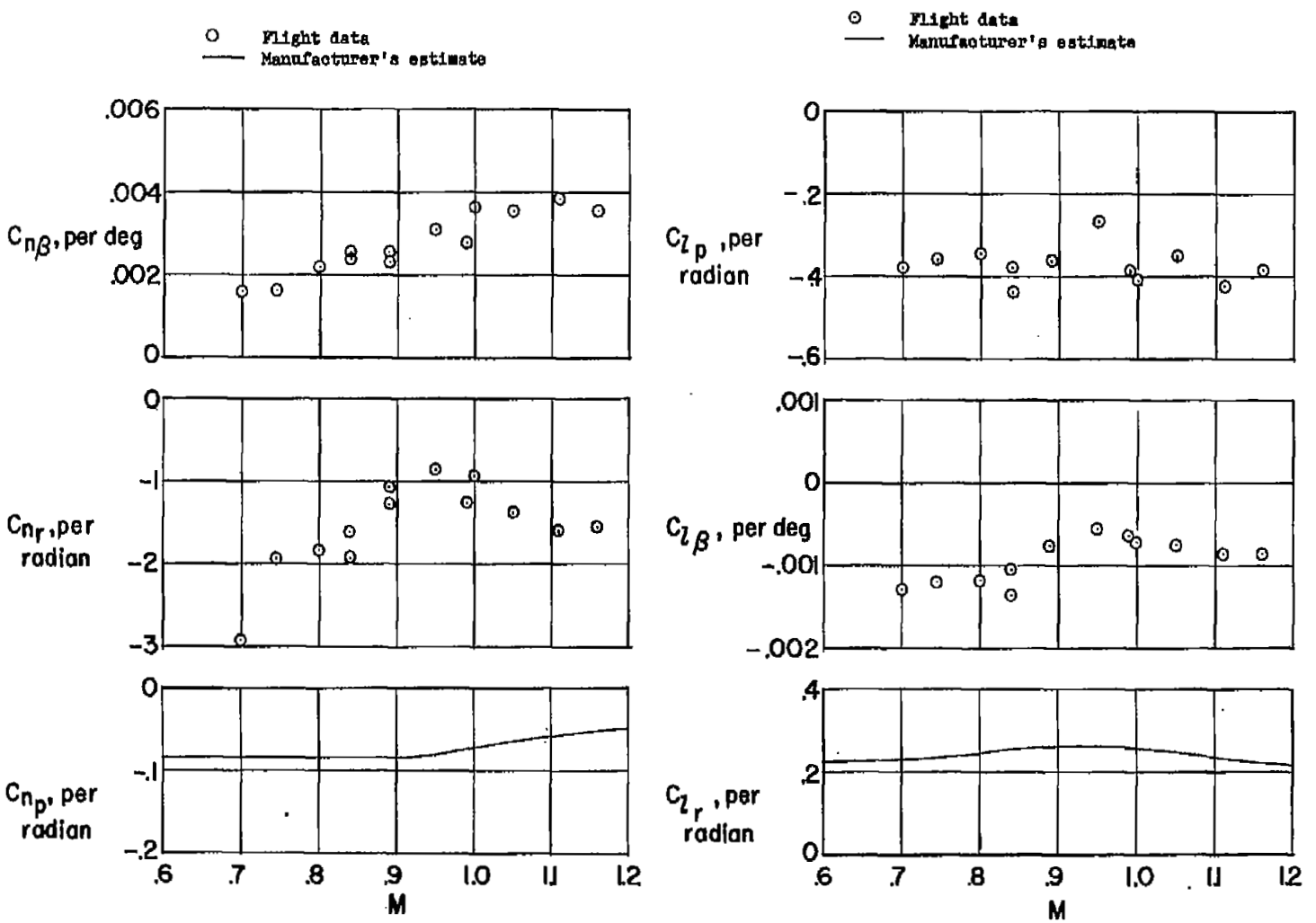

Figure 19.- Lateral stability parameters as a function of Mach number determined from oscillations following abrupt rudder-pulse maneuvers.

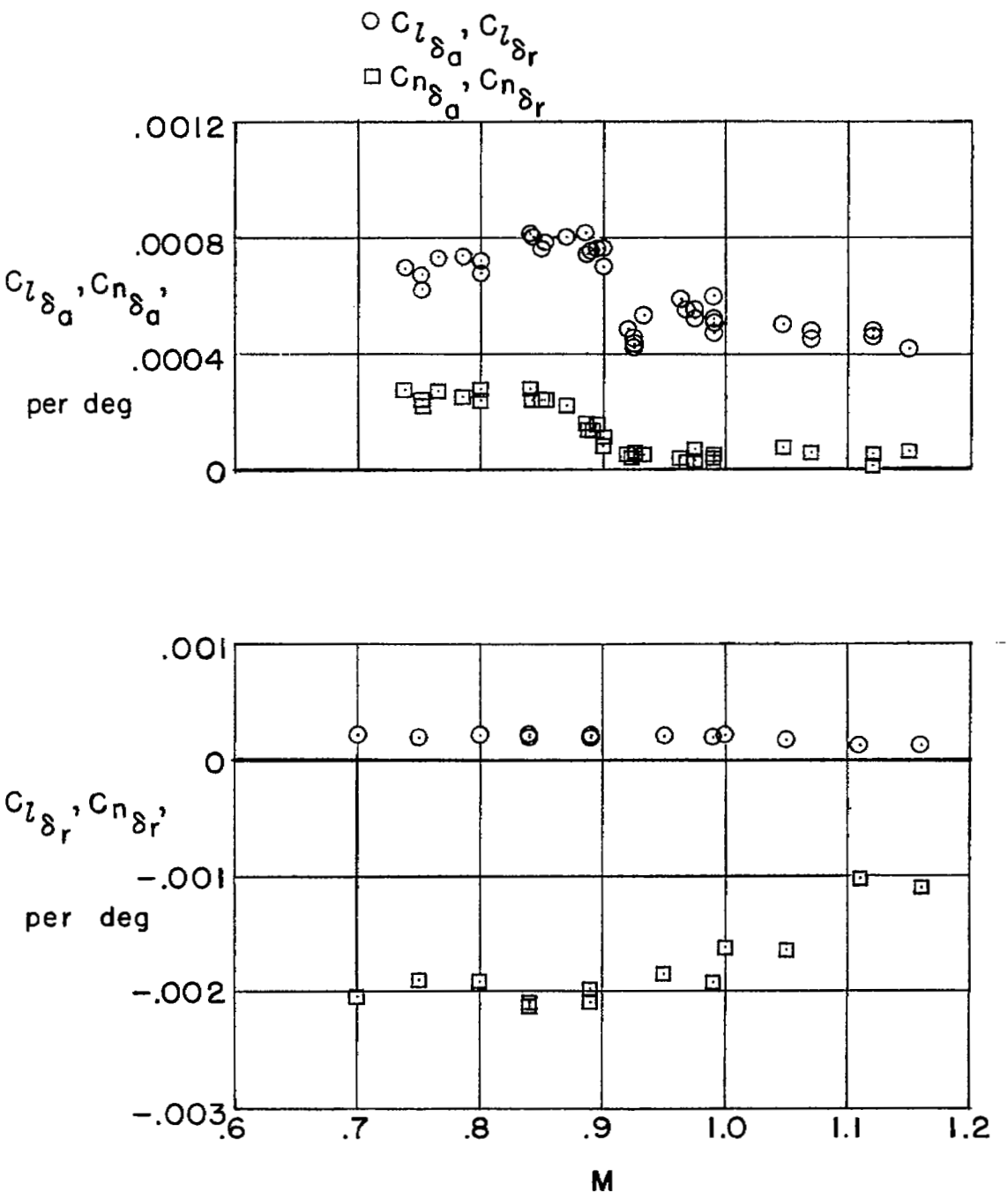

Figure 20.- Aileron and rudder control effectiveness parameters as a function of Mach number.

[redacted]

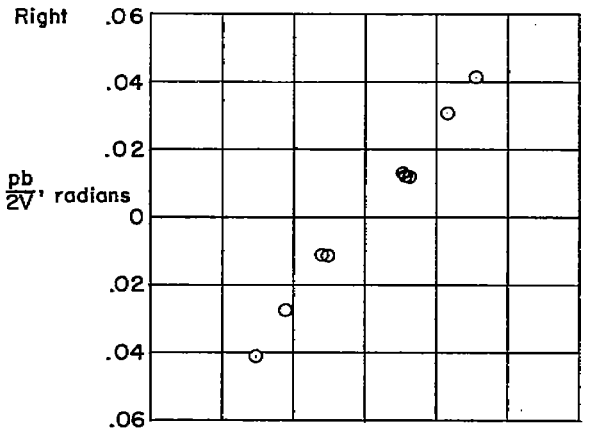

(a) M = 0.75 ± 0.02.

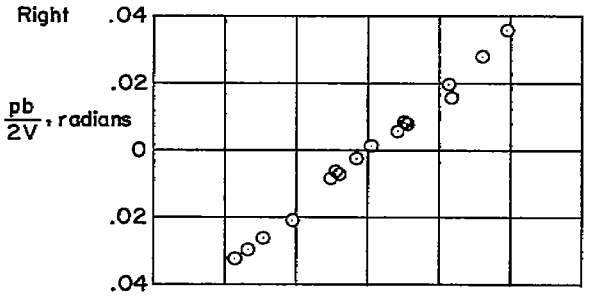

(b) M = 0.98 ± 0.02.

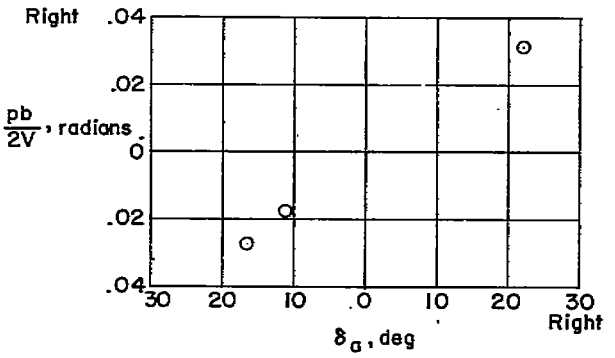

(c) M = 1.13 ± 0.02.

Figure 21.- Representative variations of wing-tip helix angle as a function of aileron deflection.

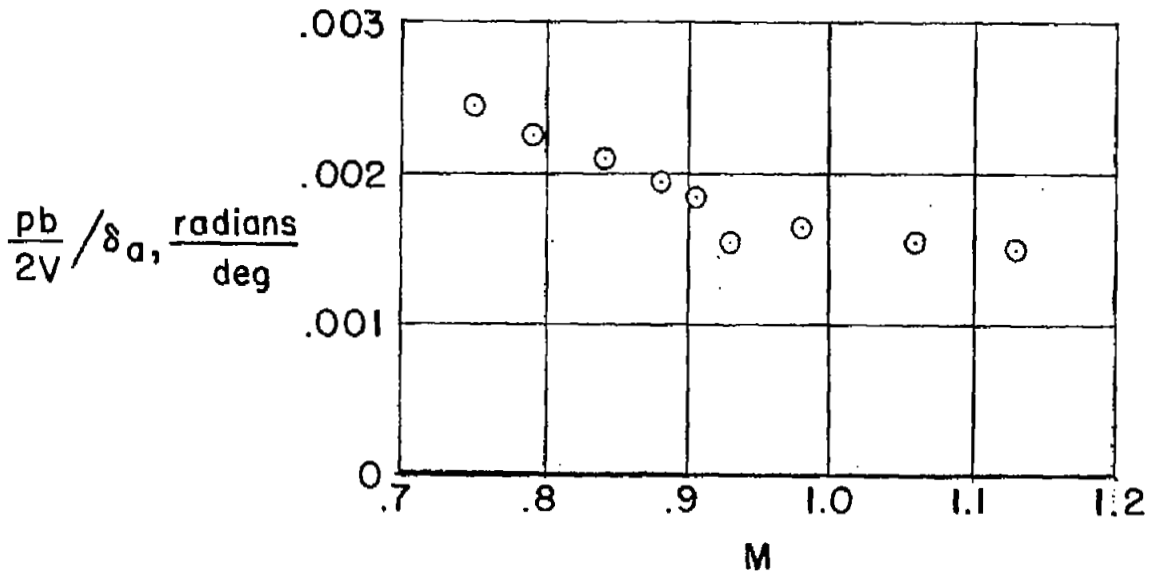

Figure 22.- Variation of apparent aileron effectiveness parameter per degree of aileron deflection as a function of Mach number.

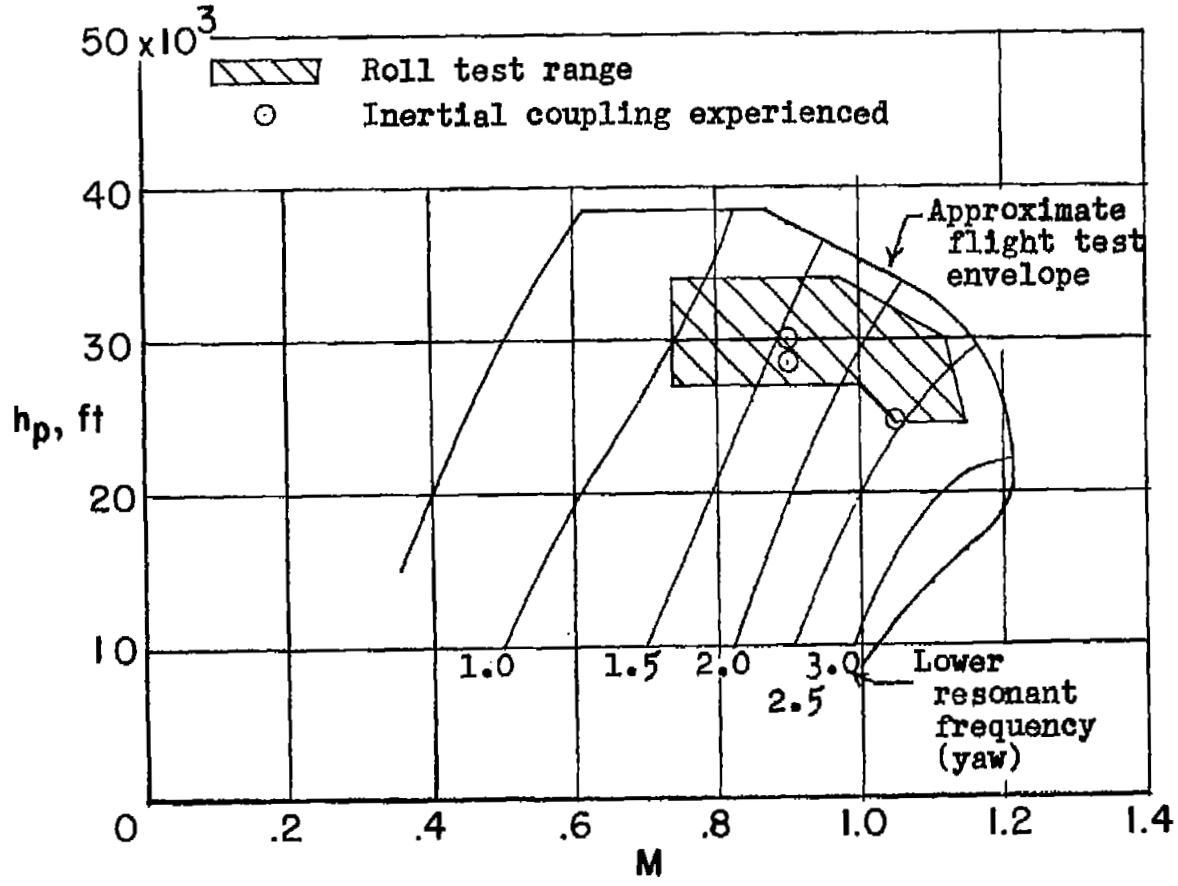

Figure 23.- Approximate flight test envelope of the X-3 research airplane, showing lines of constant lower resonant frequency (yaw) and conditions at which inertial coupling was experienced in flight.